

1 ~~Southern outlet of the Northeast Greenland Ice Stream, NE~~
2 ~~Greenland: post-Last Glacial Maximum response to climate~~
3 ~~warming—A high-Arctic inner shelf–fjord system from the Last~~
4 ~~Glacial Maximum to the Present: Bessel Fjord and SW Dove~~
5 ~~Bugt, NE Greenland~~

6 Authors: Kevin Zoller¹; Jan Sverre Laberg¹; Tom Arne Rydningen¹, Katrine Husum² & Matthias
7 Forwick¹

8 ¹Department of Geosciences, UiT The Arctic University of Norway, Box 6050 Langnes, NO-
9 9037 Tromsø, Norway ²Norwegian Polar Institute, Box 6606 Langnes, NO-9296 Tromsø,
10 Norway

11 *Correspondence to:* Kevin Zoller (kevin.zoller3@gmail.com)

12 **Abstract**

13 The Greenland Ice Sheet (GrIS) responds rapidly to the present climate, therefore, its response
14 to the predicted future warming is of concern. To learn more about [the impact of future climatic](#)
15 [warming on the ice sheet](#) ~~this~~, decoding its behavior during past periods of warmer than present
16 climate is important. However, due to the scarcity of marine studies reconstructing ice sheet
17 conditions on the Northeast Greenland shelf and adjacent fjords, ~~including the position of the ice~~
18 ~~sheet over marine regions~~, the timing of the deglaciation ~~over marine regions~~, and its
19 connection to forcing factors ~~including the Holocene Thermal Maximum (HTM) on NE~~
20 ~~Greenland~~ remain poorly constrained. ~~This includes data collected in fjords that encompass the~~
21 ~~Holocene Thermal Maximum (HTM), a period in which the climate was warmer than it is at~~
22 ~~present~~. This paper aims to use bathymetric data and the analysis of sediment gravity cores to
23 enhance our understanding of ice dynamics of the GrIS ~~in a fjord and inner shelf environment~~
24 ~~near the southern outlet of the Northeast Greenland Ice Stream (NGIS)~~, as well as give insight
25 into the timing of deglaciation and provide a palaeoenvironmental reconstruction of
26 southwestern Dove Bugt and Bessel Fjord since the Last Glacial Maximum (LGM). The swath
27 bathymetry data displayed in this study is the first time the bathymetry for Bessel Fjord has
28 become available. North-south oriented glacial lineations, and the absence of pronounced
29 moraines in southwest Dove Bugt, an inner continental shelf embayment (trough), suggests the
30 southwards and offshore flow of the southern branch of the [Northeast Greenland Ice Stream](#)
31 ~~(NEGIS)~~, Storstrømmen. Sedimentological data suggests that an ice body, theorized to be the
32 ~~NEGIS~~, may have retreated from the region slightly before ~11.42 ka ~~cal~~ BP ~~(in the Preboreal~~
33 ~~period)~~. The seabed morphology of Bessel Fjord, a fjord terminating in southern Dove Bugt,
34 includes numerous basins, separated by thresholds. The position of basin thresholds, which
35 include some recessional moraines, suggest that the GrIS had undergone multiple halts or
36 readvances during deglaciation, ~~likely during one of the cold events identified in the Greenland~~
37 ~~Summit temperature records~~ (Kobashi et al., 2017). A minimum age of 7.12 ka ~~cal~~ BP is
38 proposed for the retreat of ice ~~through the fjord~~ to or west of its present-day position in the
39 Bessel Fjord catchment area. This suggests that the GrIS retreated from the marine realm in
40 early Holocene, around ~~the time of~~ the onset of the Holocene Thermal Maximum in this region,
41 a period when the mean July temperature according to Bennike et al., (2008) was at least 2-3
42 °C higher than at present, and remained at or west of this onshore position for the remainder of

43 the Holocene.- The transition from predominantly mud to muddy sand layers in a mid-fjord core
44 at ~4 ka cal BP may be the result of increased sediment input from nearby and growing ice
45 caps. This shift may suggest that in the late Holocene (Meghalayan), a period characterized by
46 a temperature drop to modern values, ice caps in Bessel Fjord fluctuated with greater sensitivity
47 to climatic conditions than the NE sector of the GrIS.

48 1. Introduction

49 Ice mass loss from the Greenland Ice Sheet (GrIS) has accelerated during the 21 century,
50 making it the current largest individual contributor to sea level rise (King et al., 2020). This
51 introduction of a substantial quantity of fresh water may have ramifications for global ocean
52 circulations as well as the climate (Rahmstorf et al., 2015). Approximately 12% of the ice from
53 the GrIS is transported to the coast through the Northeast Greenland Ice Stream (NEGIS) (Khan
54 et al., 2014; Joughin et al., 2001) (~~Larsen et al., 2018~~) and therefore has a substantial impact on
55 the mass balance of the ice sheet and a potential to contribute to sea level rise.- Currently, two
56 of the three marine terminating outlet glaciers that are supplied by the NEGIS are in retreat
57 (Mouginot et al., 2015), where the southernmost branch, Storstrømmen in Dove Bugt (Figs. 1a
58 & 1b), is currently in a building phase following a 1978-1984 surge (Khan et al., 2014; Reeh et
59 al., 1994; ~~Larsen et al., 2018~~). While there are numerous modern studies on the current state of
60 the NEGIS during the past decades to century, there is a scarcity of data concerning the
61 position and dynamics of the ice stream, and other local Northeast Greenland outlet glaciers, on
62 a multi-century to millennia scale over marine regions. Considering that the global mean
63 temperature is expected to continue to rise (Stocker et al., 2013), and that the Arctic will
64 experience an amplification effect (Cohen et al., 2014), looking to the past, especially during
65 warmer than present periods (i.e., the Holocene Thermal Maximum (HTM)), may provide an
66 important insight into the future behavior of the ice sheet.

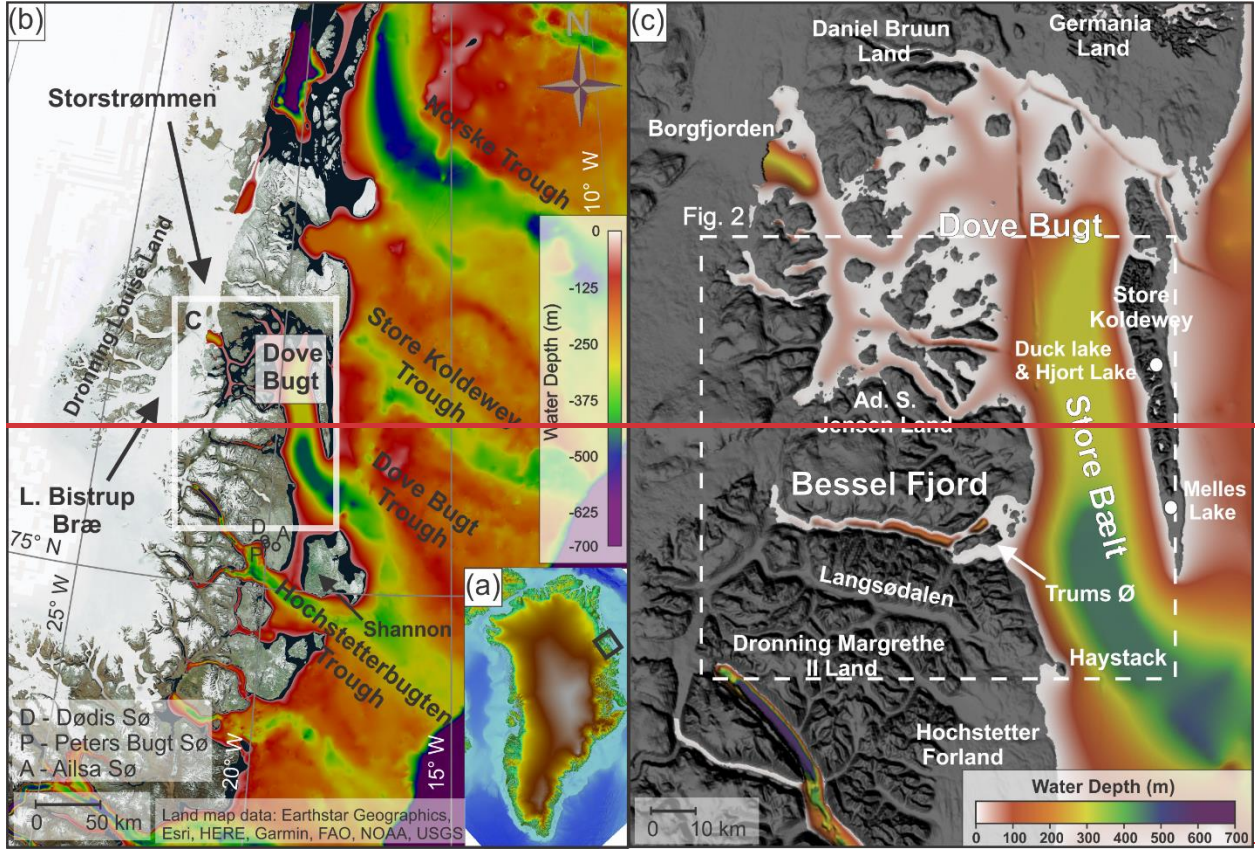
67 Marine studies have found evidence for past advancement and retreat of the GrIS and NEGIS
68 along the continental shelf offshore Northeast Greenland (Evans et al., 2009; Winkelmann et al.,
69 2010; Arndt et al., 2015, 2017; Laberg et al., 2017; Arndt, 2018; Olsen et al., 2020; Syring et al.,
70 2020; Davies et al., 2022; Hansen et al., 2022; Jackson et al., 2022). (~~Evans et al., 2009;~~
71 ~~Winkelmann et al., 2010; Arndt et al., 2015, 2017; Laberg et al., 2017; Arndt, 2018; Olsen et al.,~~
72 ~~2020~~).-Geomorphological findings in Store Koldewey Trough (~76°N), a major shelf trough
73 northeast of the study area (Fig. 1b), suggests that the ice sheet may have reached the shelf
74 break in this area during the LGM (Last Glacial Maximum) (Laberg et al., 2017; Olsen et al.,
75 2020).-Further north (~79.4°N), the shelf break is interpreted as being ice free during the LGM
76 (Rasmussen et al., 2022), an area where the ice front had its maximum LGM position at the
77 outer shelf according to (Arndt et al., (2017)). ~~A but a~~ concise understanding of the timing and
78 dynamics of the ice sheet ~~and ice stream over coastal and fjord regions~~ the NE Greenland shelf
79 during the subsequent deglaciation of the marine realm remains to be established as very few
80 dated cores have been recovered. Terrestrial dating (e.g., cosmogenic nuclide dates and lake
81 studies) has provided further insight into when terrestrial regions had become deglaciated, and
82 how the climate has changed in these areas_- (Wagner et al., 2008; Klug et al., 2009a; Schmidt
83 et al., 2011; Briner et al., 2016; Björck and Persson, 1981; Björck et al., 1994; Skov et al.,
84 2020).- (e.g., Björck and Persson, 1981; Björck et al., 1994; Wagner et al., 2008; Klug et al.,
85 2009a; Schmidt et al., 2011; Briner et al., 2016; Skov et al., 2020; Larsen et al., 2020).
86 However, only recently has a proper terrestrial data been integrated ~~edion~~ with marine data to

87 establish a detailed deglaciation chronology of the shelf, coastal and fjord regions (Davies et al.,
88 2022; Larsen et al., 2022) ~~of the deglaciation is still pending.~~

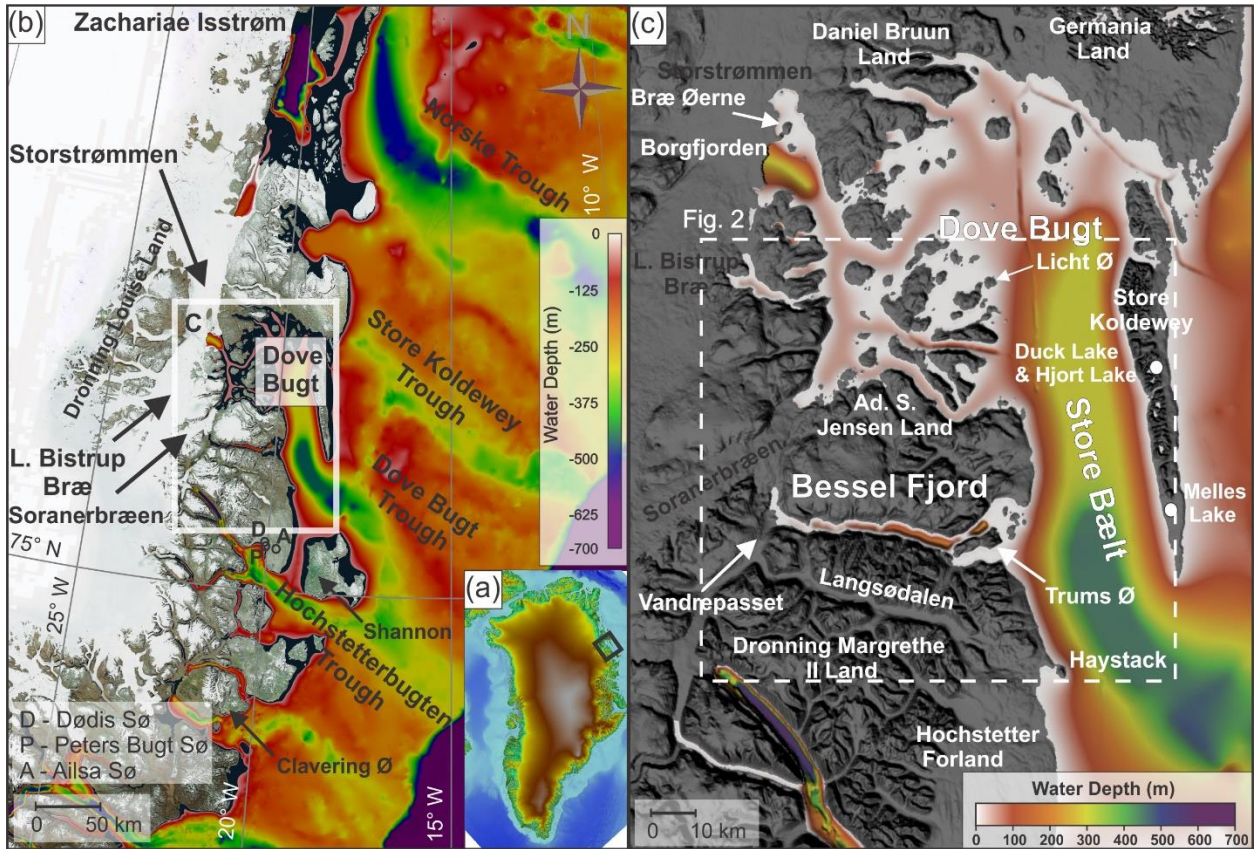
89 Swath bathymetry and gravity cores data from southwestern Dove Bugt (i.e., Store Bælt) and
90 Bessel Fjord (Fig. 1), presented for the first time in this study, has been used to further refine
91 our understanding of how the GrIS ~~and NGIS~~ responded to changes in palaeoclimatic
92 conditions from the LGM through the Holocene, including the HTM. Through this analysis we
93 aim to reconstruct regional ice dynamics from both full-glacial conditions and during overall
94 retreat and put our findings into the larger context of the dynamics of the Northeast Greenland
95 Ice Sheet during these periods. Additionally, this study aims to refine our understanding about
96 the timing of deglaciation over marine areas and compare findings to nearby terrestrial regions
97 including the Store Koldewey island and Hochstetter Forland/Shannon Ø. Results will also
98 contribute to our understanding of palaeoenvironmental conditions throughout the Holocene for
99 the NE Greenland fjords and inner shelf areas.

100

101



102



103 Figure 1. (a) An image of Greenland, using IBCAO 4.0 400x400m (Jakobsson et al., 2020), with a black box
104 surrounding the study area. (b) Bathymetry of ~~northern-E~~Northeast Greenland displayed using IBCAO 4.0 200x200m
105 data (Jakobsson et al., 2020) and land is displayed using a World Imagery satellite image (~~Earthstar Geographics-~~
106 ~~Esri~~)(Earthstar Geographics, Esri, HERE, Garmin, FAO, NOAA, USGS) made available through GlobalMapper. The
107 white box surrounds the position of Fig. 1c. (c) Bathymetry of Dove Bugt and Bessel Fjord and surrounding land
108 areas displayed using the IBCAO 4.0 200x200m data (Jakobsson et al., 2020). Locations mentioned in the text are
109 labelled here. The position of Fig. 2 is within the white dashed box.

110 2. Regional Setting and Environmental History

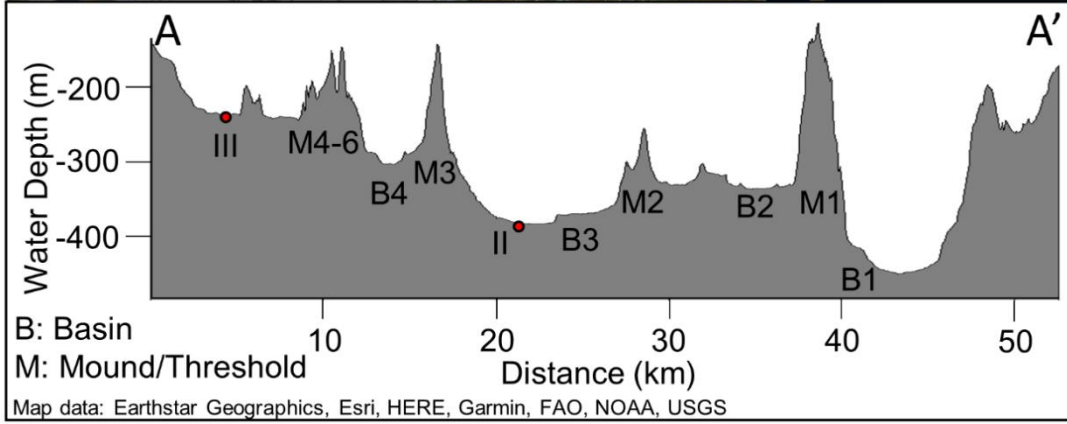
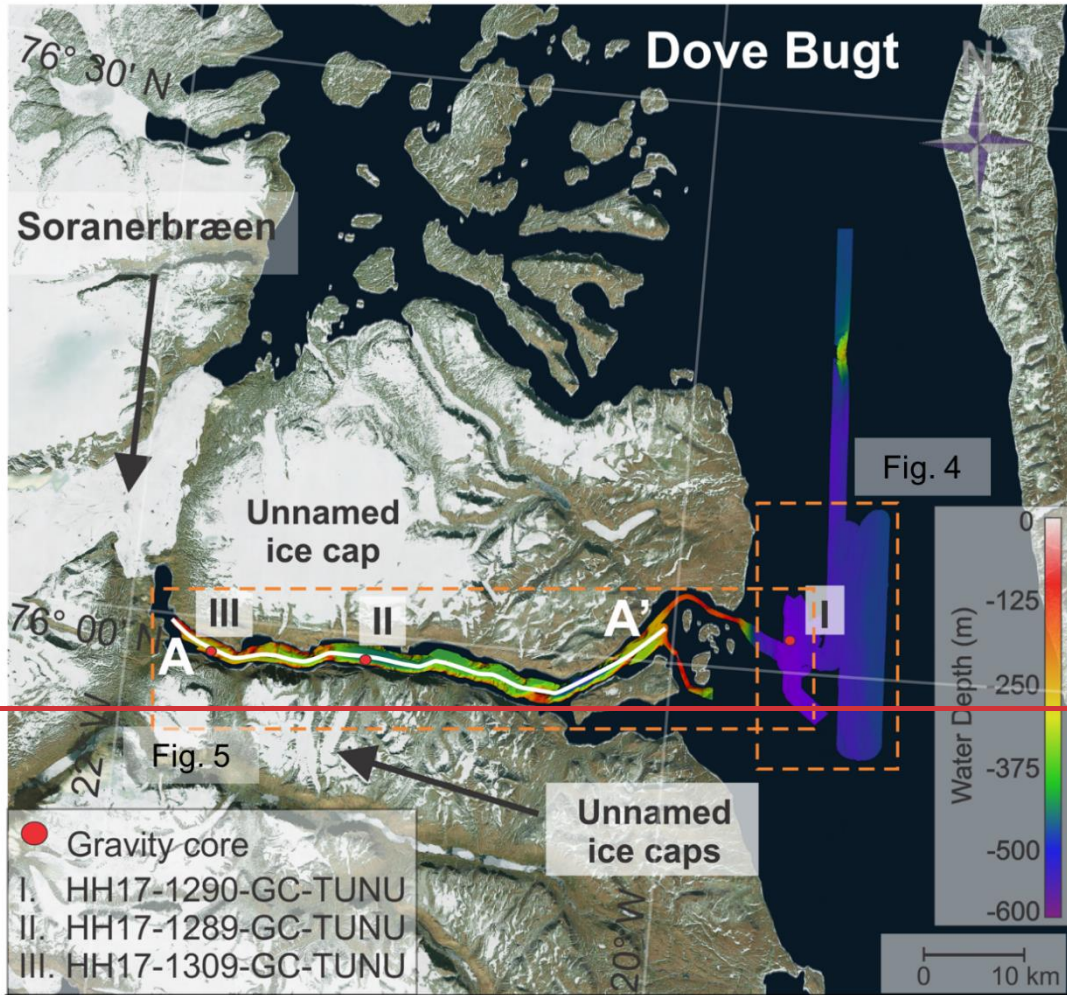
111 Bessel Fjord is a west-east running fjord between Adolf S. Jensen Land and Dronning
112 Margrethe II Land (Fig. 1c). The western end of the fjord contains the southern outlet glacier
113 Soranerbræen, which also has a second outlet to the north in a tributary fjord to inner Dove Bugt
114 (Fig. 2). Several ice caps are positioned across the length of the fjord (Figs. 2 & 3), some of
115 which have several generations of moraines and glaciofluvial outlets that enter the fjord.
116 Colluvial fans and rivers have been observed across the length of the fjord in satellite images
117 and while surveying the fjord. Multiple islands are located at the entrance of Bessel Fjord, the
118 largest of which, Trums Ø, splits the entrance into two main inlets (Figs. 1c & 2). From the
119 termination of Soranerbræen to the entrance of the fjord measures ~60 km in length. The width
120 of the fjord ranges from 1.8 to 3.7 km.

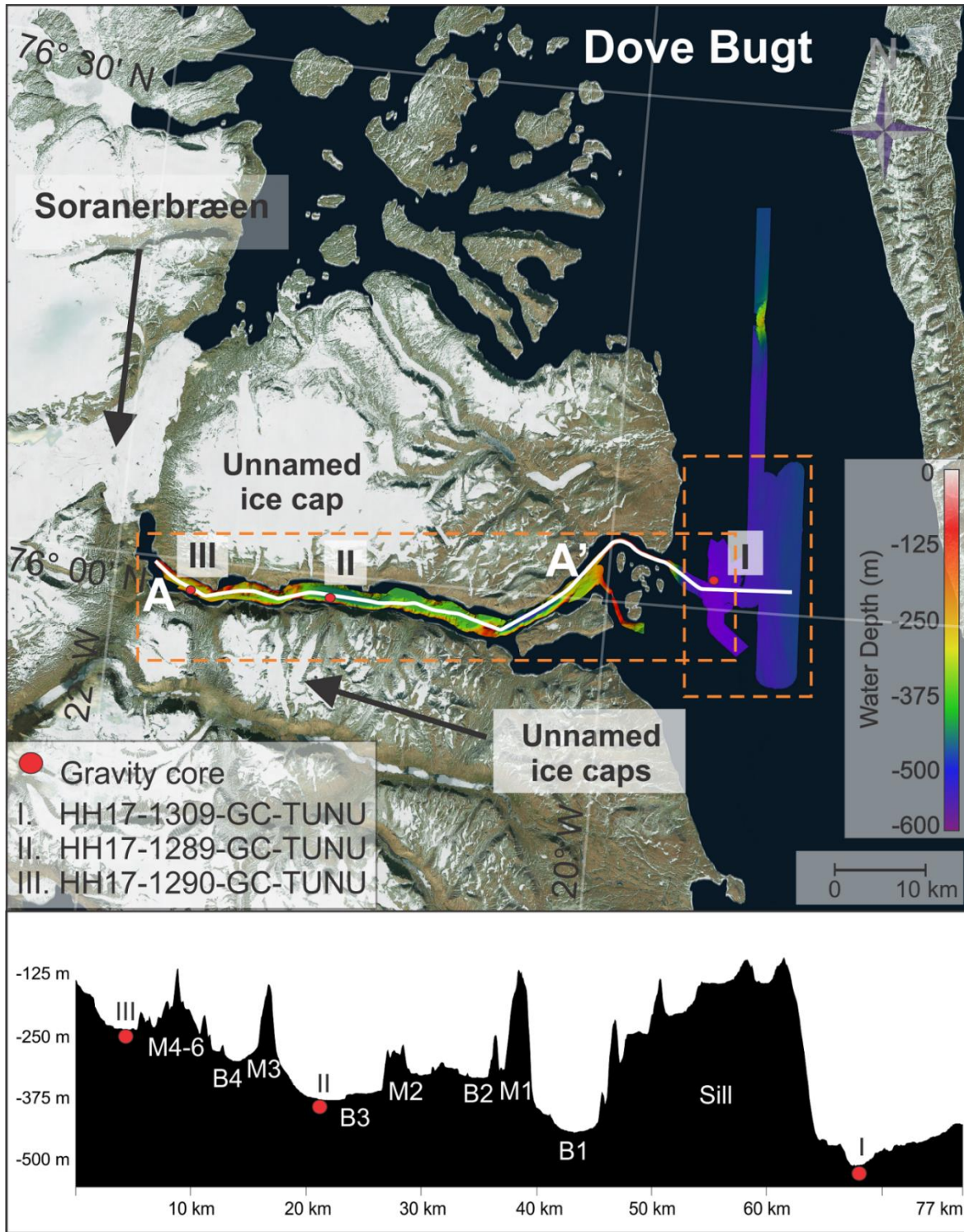
121 To the west of Bessel Fjord and Soranerbræen is the larger glacier L. Bistrup Bræ, which flows
122 northwards and has an outlet in Borgfjorden, another tributary fjord to inner Dove Bugt (Fig 1).
123 Here it is confluent with the southward flowing NEGIS outlet glacier, Storstrømmen (Rignot et
124 al., 2022). Studies of modern Soranerbræen, L. Bistrup Bræ and Storstrømmen suggest that
125 they all have separate drainage basins (Krieger et al., 2020). Dove Bugt is an embayment
126 situated east of the southernmost outlets of the NGIS, Storstrømmen and L. Bistrup Bræ (Fig.
127 4b). Storstrømmen and L. Bistrup Bræ are two of the largest surge-type glaciers in the world
128 (Higgins, 1991) with a surge periodicity of approximately 70 years (Mouginot et al., 2018).
129 These two glaciers flow north and south, respectively, around the nunatak complex of Dronning
130 Louise Land and merge in Borgfjorden (Fig 1b & 1c; (Mouginot et al., 2018).

131 Bathymetry of inner Dove Bugt and tributary fjords has revealed that there are no natural large
132 passageways for the warm, salty, subsurface Atlantic Intermediate Water to impact these
133 glaciers at present, therefore it has been suggested that ocean waters do not play a large role in
134 the evolution of Storstrømmen, L. Bistrup Bræ and the northern outlet of Soranerbræen, and
135 that their grounding line retreat is mostly caused by ice thinning (Rignot et al., 2022). The
136 elongated island of Store Koldewey to the east of Dove Bugt largely shelters the embayment
137 from the East Greenland Current. South of the bay is the sound Store Bælt, which is an outlet to
138 the Greenland Sea.

139 West of Store Bælt, between Adolf S. Jensen Land and Dronning Margrethe II Land, is the
140 west-east running Bessel Fjord (Fig. 1c). The western end of the fjord contains one of the two
141 outlets of Soranerbræen, an outlet glacier that also connects to Dove Bugt to the north (Fig. 2).
142 Several ice caps are positioned across the length of the fjord (Fig. 2 & 3), some of which have
143 several generations of moraines and glaciofluvial outlets that enter the fjord. Colluvial fans and
144 rivers have been observed across the length of the fjord in satellite images and while surveying
145 the fjord. Multiple islands are located at the entrance of Bessel Fjord, the largest of which,
146 Trums Ø, splits the entrance into two main inlets (Fig. 1c & 2). From the termination of

147 Mega-scale glacial lineations (MSGL) identified in Store Koldewey Trough on the continental
148 shelf have been interpreted as evidence for the expanse of this sector of the GrIS to the shelf
149 break during the LGM (Laberg et al., 2017; Olsen et al., 2020). This is further supported by the
150 presence of recessional moraines and grounding zone wedges, which suggests a complex
151 deglaciation of this part of the shelf area (Arndt et al., 2015, 2017; Laberg et al., 2017; Arndt,
152 2018; Olsen et al., 2020). Olsen et al. (2020) has suggested that deglaciation in the Store
153 Koldewey Trough may have occurred in two stages: first, an initial retreat as a result of eustatic
154 sea level rise caused by melting ice at lower latitudes (Lambeck et al., 2014), followed by a
155 melting phase driven by ocean warming. So far, the timing of the onset of the deglaciation is not
156 known. Across the GrIS, deglaciation is believed to be asynchronous, with factors such as
157 topography and local ice dynamics playing a large role with ice retreat in conjunction with
158 climate change (Bennike & Björck, 2002; Funder et al., 2011; Ó Cofaigh et al., 2013; Hogan et
159 al., 2016).





161

162 *Figure 2. Study area with the bathymetric data showing the locations of the sediment cores presented in this study.*
 163 *The lower panel is a profile along the length of Bessel Fjord, A-A'. Sediment cores are labelled I, II and III. Satellite*
 164 *image is displayed using a World Imagery satellite image ([Earthstar Geographics](#) | [Esri](#)) ([Earthstar Geographics](#), [Esri](#),*
 165 *[HERE](#), [Garmin](#), [FAO](#), [NOAA](#), [USGS](#)) made available through GlobalMapper.*

166



167

168 *Figure 3. Image of an ice lobe from an ice cap near gravity core HH17-1289-GC-TUNU. Two sets of coarse-grained*
 169 *terminal morainal ridges are indicated by numbers and arrow. See Fig. 6b for the position of the modern ice lobe. The*
 170 *photograph was taken by Torger Grytå on a 2017 TUNU cruise.*

171 ~~Soranerbræen to the island of Trums Ø the fjord measures approximately 47 km in length. The~~
 172 ~~width of the fjord ranges from 1.8 to 3.7 km.~~

173 ~~Mega-scale glacial lineations (MSGL) identified along the continental shelf have been~~
 174 ~~interpreted as evidence for the expanse of the GrIS to the shelf break during the LGM at this~~
 175 ~~latitude (Laberg et al., 2017; Olsen et al., 2020). This is further supported by the presence of~~
 176 ~~recessional moraines and grounding zone wedges identified across the continental shelf of~~
 177 ~~Northeast Greenland, which suggests a complex deglaciation of the shelf area. Across the~~
 178 ~~GrIS, deglaciation is believed to be asynchronous, with factors such as topography and local ice~~
 179 ~~dynamics playing a large role with ice retreat in conjunction with climate change. Olsen et al.~~
 180 ~~(2020) has suggested that deglaciation in the northeast may have occurred in two stages: first,~~
 181 ~~an initial retreat as a result of eustatic sea level rise caused by melting ice at lower latitudes~~
 182 ~~(Lambeck et al., 2014), followed by a melting phase driven by ocean warming.~~

183 A recent study by Jackson et al. (2022) of the inner shelf east of the Clavering Ø (~74° N; Fig.
 184 1b) indicated that during the late Younger Dryas, this sector of the GrIS had reached a more
 185 landward position, in conformity with Funder et al. (2021). During this period the inner shelf
 186 bottom water was characterized by anomalously high temperatures, interpreted to have played
 187 a role in the ice retreat and leading to the termination of the Younger Dryas stadial. This was
 188 followed by the onset of the East Greenland Current, as seen from cooler bottom water from the
 189 Early Holocene on (Jackson et al., 2022).

190 Further north, east of marine terminating glacier Zachariae Isstrøm (~78° 30N; Fig. 1b), the
191 deglaciation of the NEGIS from the inner shelf was found to have occurred as early as 12.5 ka
192 cal BP, likely before 13.4 ka cal BP. Here, inflow of warmer water (Atlantic Water) may have
193 played a role. This part of the shelf was covered by an ice shelf from 13.4 to 11.2 ka cal BP
194 (including the Younger Dryas), retreating and leading to open water conditions from the earliest
195 Holocene; 11.2-10.8 ka cal BP, before readvancing from 10.8 to 9.6 ka cal BP, finally retreating
196 from 9.6 to 7.9 ka cal BP. At 7.9 ka cal BP there was a drastic shift in ocean circulation at this
197 site with a sharp decline in Atlantic Water corresponding to an increase in Polar Water influx
198 (Davies et al., 2022). Pados-Dibattista et al. (2022), studying another core from the NE
199 Greenland shelf (more seaward, in a mid-shelf position north of the Norske Trough at ~79°N),
200 found that during the early Holocene (9.4 to 8.2 ka cal BP), the East Greenland Current was
201 highly stratified with cold surface water overlying warm Atlantic subsurface water. Following the
202 8.2 ka event, the interval from 8.2 to 6.2 ka cal BP was followed by the warmest Holocene
203 bottom water conditions on the shelf. Afterwards, conditions returned to those seen prior to 8.2
204 ka cal BP due to increased Polar Water transport strengthening the East Greenland Current.

205 Terrestrial studies of Dronnings Margrethe II Land, Germania Land and adjacent areas have
206 identified a complex assortment of moraines that are believed to have formed during the Kap
207 Mackenzie, Muschelbjerg, Nanok I and Nanok II stadials (Hjort, 1979, 1981; Hjort and Björck,
208 1983; Björck et al., 1994; Landvik, 1994). The exact ages of these stadials remain unclear
209 (Table 1), yet ~~(Larsen et al., (2022))~~ ~~Vasskog et al. (2015)~~ suggests that the Nanok-stadial
210 moraines found in Store Koldewey formed synchronously with the Milne Land moraines of
211 Scoresby Sund which date to the Allerød to early Younger Dryas and Preboreal time (Kelly et
212 al., 2008; Levy et al., 2016). ~~Milne Land moraines (referred to as G-II) formed during the late~~
213 ~~Younger Dryas (~12 ka BP) (Table 1).~~

214
215
216
217
218
219
220
221
222
223
224
225
226
227

228 *Table 1. Previously published stadial information for the Dove Bugt region as well as age estimates used in this*
 229 *study.*

Stadials	Studies					Age estimate used in this study
	<i>Hjort & Björck (1983)</i>	<i>Funder et al., (1998)</i>	<i>Kelly et al. (2008)</i>	<i>Vasskog et al. (2015)</i>	<i>Larsen et al. (2022)</i>	
<i>Nanok II</i>	10.1-9.5 ka cal BP	Preboreal (ending at ca. 9.7 ka cal BP)	Younger Dryas and Early Holocene (13-11.6 ka cal BP (G-III), 11.7-10.6 ka cal BP (G II))	Close to Bølling– Allerød transition, and late Younger Dryas (~14 ka cal BP (G III), ~12 ka cal BP (G-II))	Preboreal	Preboreal
<i>Nanok I</i>	Older than 14 ka cal BP, possibly between 15 and 19 ka cal BP				Late Allerød to early Younger Dryas	Late Allerød to early Younger Dryas
<i>Nanok 0</i>		~48 ka (Hjort, unpublished data)				?
<i>Muschelbjerg</i>	Saalian (or older)?					Saalian (or older)?
<i>Kap Mackenzie</i>	Saalian (or older)?					Saalian (or older)?

230
231

232 The position of striations on Store Koldewey and lateral moraines on coastal slopes between
 233 Bessel Fjord and Haystack have been interpreted as evidence for ice flowing out of Dove Bugt
 234 and Bessel Fjord during the Muschelbjerg stadial, southwards through Store Bælt and turning
 235 eastwards around the southernmost mountains of Store Koldewey (Hjort, 1981). Early studies of
 236 the region noted glacial and glaciofluvial deposits (e.g. moraine plateaux, terminal moraines,
 237 eskers and sandurs) on Hochstetter Forland that are believed to have formed during this period
 238 (Hjort, 1979, 1981).

239 Lateral moraines and glacial striations oriented along the axis of Langsodal (also referred to as
 240 Langsødal; Fig. 1c), a nearby valley south of and sub-parallel to Bessel Fjord, have been
 241 interpreted as evidence for glacial confinement within the valley during an undifferentiated
 242 Nanok stadial (Hjort 1979; Hjort, 1981). This differs from striations that have also been identified
 243 in the valley along more weathered surfaces that are oriented in a southwestern direction (Hjort,
 244 1979).

245 On terrestrial areas, cosmogenic nuclide dates collected from Store Koldewey suggest that the
246 region was deglaciated by 12.7 ka BP (Skov et al., 2020). The outer coastal regions of North
247 and Northeast Greenland are believed to have been deglaciated between 12.8 and 9.7 ka cal
248 BP and present ice positions were reached between 10.8 to 5.8 ka cal BP (Larsen et al., 2022).
249 Cosmogenic nuclide dates from Store Koldewey, first collected by Håkansson et al. (2007), and
250 later Skov et al. (2020) and Larsen et al. (2022), suggest that ice retreated from the continental
251 shelf and reached the upper and lower sections of the island by 12.3 and 12.7 ka cal BP,
252 respectively. In contrast, Biette et al. (2020) found evidence of the deglaciation of Clavering Ø at
253 16.2 ka cal BP, with readvances at 11.3, 10.8, 3.3, 1.2 and 0.37 ka cal BP. Additional
254 cosmogenic nuclide findings indicate that Trums Ø, in outer Bessel Fjord, may have become
255 deglaciated around 12.6 ka cal BP and Vandrepasset, onshore inner Bessel Fjord, by 8.6 ka cal
256 BP (Larsen et al., 2022).

257 Findings from macrofossil remains (Bennike & Björck, 2002) and lacustrine sedimentary records
258 (Cremer et al., 2008) suggest that coastal regions were deglaciated in a ~1500 year span after
259 the start of the Holocene (Klug et al., 2016). To the north of Store Koldewey, a minimum date
260 for deglaciation in Germania Land of 9.5 ka cal BP has been proposed (Landvik, 1994),
261 whereas to the south in southern Dronning Margrethe II Land, a minimum date of 11.2 ka cal BP
262 has been suggested (Bennike & Weidick, 2001).

263 Lake studies on aquatic organisms at BjörckDuck Lake and Hjort Lake on Store Koldewey (Fig.
264 1c) indicate that the island was at its warmest between ~8 and 4 ka cal BP, (Wagner et al.,
265 2008; Klug et al., 2009; Schmidt et al., 2011), although findings from Melles Lake (Fig. 1c)
266 suggest that the earliest onset of warmth during the Holocene may have occurred at ~ 10 ka cal
267 BP (Klug et al., 2009; Briner et al., 2016). On Hochstetter Forland (Fig. 1c), pollen assemblages
268 from Dødis Sø, Peters Bugt Sø and Ailsa Sø suggest that the temperatures were at their
269 highest between 8.8 and 5.6 ka cal BP (Björck & Persson, 1981; Björck et al., 1994). These
270 findings indicate that the HTM was not uniform across East Greenland, as also described by
271 Briner et al. (2016).

272 To the south, offshore the Kejser Franz Josef fjord system (~73°N), a detailed biomarker record
273 finds this part of the shelf dominated by seasonal sea ice throughout the late Holocene (<~5 ka
274 cal BP) and extended concentrations from 5.2 to 2.2 and 1.3 to present. Short-term variability
275 was also seen for this area for the last 2.2 ka cal BP, corresponding to the climatic events of this
276 period (Kolling et al., 2017).

277 **3. Material and Methods**

278 Swath bathymetry and three sediment cores were collected in southwestern Dove Bugt and
279 Bessel Fjord during an expedition aboard RV *Helmer Hanssen* of UiT The Arctic University of
280 Norway in September 2017, being part of the TUNU program (Fig. 2; Christiansen, 2012). The
281 swath bathymetry data was obtained using a Kongsberg Maritime Simrad EM 302 multibeam
282 echo sounder. It was gridded using Petrel software, and geomorphological interpretations were
283 made using Global Mapper 18. Surfaces were developed using a 5x5m grid cell size while a
284 surface created from an International Bathymetric Chart of the Arctic Ocean (IBCAO) dataset
285 4.0 with a 200x200m grid cell size (Jakobsson et al., 2020).

286 Two soft sediment gravity cores were retrieved from Bessel Fjord (HH17-1289-GC-TUNU &
287 HH17-1290-GC-TUNU) and one southwest of Dove Bugt in the sound Store Bælt (HH17-1309-

288 GC-TUNU) (Fig. 2 & Table 2). Prior to splitting the cores, physical properties were measured
 289 using a GEOTEK Multi Sensor Core Logger (MSCL-S). The cores were placed in the laboratory
 290 for 24 hours prior to obtaining physical measurements to ensure that each core temperature
 291 reached equilibrium with the laboratory to avoid distorting p-wave values (Weber et al., 1997).

292 *Table 2. Information on the position, water depth and recovery length of each gravity core. Note that the core names*
 293 *are abbreviated in the text.*

Location	Inner Bessel Fjord	Mid-Bessel Fjord	Southeastern Dove Bugt
Coring station	HH17-1290	HH17-1289	HH17-1309
Latitude [N]	75° 58' 34.5907"	75° 58' 11.4928"	76° 01' 34.0387"
Longitude [W]	21° 07' 13.1055"	21° 41' 48.0278"	19° 34' 31.3190"
Water depth [m]	372	225	512
Recovery [cm]	534.5	245.5	474.55

294

295 A GEOTEK MSCL X-ray Computed Tomographic imaging machine was also used to scan the
 296 unopened core sections to create X-ray radiographic images. After each core was split and
 297 cleaned, the characteristics of the sedimentary surface were logged (i.e., structures,
 298 bioturbation, grain size, lithological boundaries, etc.), sediment color was noted using the
 299 Munsell Soil Color Chart and lithofacies were assigned based on Eyles et al. (1983)
 300 classification system. X-ray fluorescence (XRF) data ([not published here](#)), as well as colored
 301 images of the core sections, were then obtained using an Avaatech XRF core scanner. ~~Ca/Fe
 302 elemental ratios have been added to core logs as this ratio can be used to distinguish between
 303 biogenic carbonate and detrital clay content (Rothwell et al., 2006). It is worth noting that
 304 sediment cores collected near areas of terrestrial runoff have the potential to introduce non-
 305 biogenic calcium into the sampled sediment which can dilute the signal of the biogenic
 306 carbonate. While runoff from glaciers and rivers have the potential to impact the cores in Dove
 307 Bugt and Bessel Fjord, what is known about the chemical composition of the surrounding rocks
 308 in Bessel Fjord (Henriksen and Higgins, 2009) suggests that the introduction of terrestrial
 309 calcium would only likely minimally impact Ca/Fe ratios. Therefore, while it is important to
 310 consider the potential influence of terrestrial calcium, at this time their impact is believed to be
 311 negligible.~~

312 Molluscs and benthic foraminifera were recovered from each core for the purpose of
 313 radiocarbon dating ~~of lithofacies boundaries. This was, however, not always possible due to the
 314 low content of foraminifera and molluscs in these cores which also restricted the number of
 315 dates that could be obtained.~~ Two adjacent 1 cm thick sediment slices were successfully
 316 sampled from select positions across cores HH17-1290 and HH17-1309. Samples were then
 317 wet sieved at 1 mm, 100 µm and 63 µm meshes, respectively. Benthic foraminifera from the
 318 100-µm size fraction were extracted for radiocarbon dating. Radiocarbon dating was carried out
 319 at the MICADAS radiocarbon laboratory at Alfred Wegener Institute, Helmholtz Centre for Polar
 320 and Marine Research, Germany. The radiocarbon dates were calibrated using the online
 321 version of OxCal 4.4 (<https://c14.arch.ox.ac.uk/oxcal.html#program>) and the Marine20
 322 calibration curve (Heaton et al., 2020), ~~as the calibrated 14C samples are younger than 11.5 ka~~
 323 ~~cal BP (Heaton et al., 2022). We are Calib 7.1 software (Stuiver and Reimer, 1993) applying the~~
 324 ~~MARINE13 calibration curve (Reimer et al., 2013) using and a ΔR of -10462 ± 6027 years~~
 325 ~~suggested for this region (Håkansson, 1973; Funder, 1982), in conformity with (Jackson et al.~~

326 (2022). Previously reported radiocarbon dates from this area that are relevant to our study have
327 been recalibrated using Marine20 for marine samples under 11.5 ka and IntCal20 for terrestrial
328 samples (Reimer et al., 2020). One marine sample older than 11.5 ka cal BP has also been
329 included (Table 3). We are aware that for the Arctic, including our study area, calibration of
330 marine samples by Marine20 is not recommended for samples older than 11.5 cal ka BP (see
331 (Heaton et al., (2022), therefore, this calibrated age is treated with caution.

332 A Beckman Coulter LS 13 320 Multi-Wavelength Laser Diffraction Particle Size Analyzer was
333 used to perform sediment grain size analysis. Sediment was sampled in mostly 10 cm intervals
334 across HH17-1309, where samples taken from the other two cores were selected from specific
335 positions. Samples were treated in HCl and H₂O₂ and a pre-heated VWB 18 Thermal Bath.
336 Samples were then cleaned using distilled water, placed through multiple runs through a
337 centrifuge and heated in an oven to remove water content. Approximately 0.2 grams of
338 sediment were then separated and placed in a container with 20 ml of water and moved to a
339 shaking table for over 48 hours. A few drops of Calgon were added to each sample, which was
340 then placed into a Branson 200 ultrasonic cleaner for ~7 minutes and shaken briefly before
341 being poured through a >2 mm mesh and into the particle size analyzer. Grains between the
342 size of 0.4 µm and 2000 µm were counted and underwent three separate runs. GRADISTAT
343 Excel-software was used to calculate the mean of the three runs. Sediment names used in
344 reference to this analysis are based on Folk (1954) and mean grain size from the methodology
345 published by Folk & Ward (1957).

346 4. Results

347 4.1. Seafloor landforms in SW Dove Bugt (Store Bælt)

348 4.1.1. Elongated Lineations - Glacial Lineations

349 Slightly curved sub-parallel lineations, oriented sub-parallel to the axis of Dove Bugt, are the
350 most pronounced landforms in this part of the study area. They are oriented N-NW in the south
351 and N-NE in the north (Fig. 4). The most frequently identified positive lineations (ridges) are 35-
352 50 m in width, <1-3 m in height and between 1 and 10 km in length. Length to width ratios are
353 frequently >10:1. At elevations shallower than 435 m depth, near the center of Store Bælt, the
354 lineations are wider (e.g., 60-150 m wide), and occasional merging and overlapping of lineations
355 occur (Fig. 4e). Wider lineations, often identified in the southern section of the study area (Fig.
356 4b), have also been identified with widths, lengths and heights ranging from 200-650 m, 3-8
357 km and 4.5-15 m, respectively. Length to width ratios here are 7:1 to >10:1. Some of the
358 larger lineations are superimposed by smaller lineations. Lateral ridges have also been
359 identified in clusters overprinting the lineations (Fig. 4c), where furrows have been found cross
360 cutting lineations (Fig. 4d). Lateral ridges measure 0.5 to 2 m in height and are approximately
361 45 to 250 m apart.

362

363

364

365

366

367

368

369

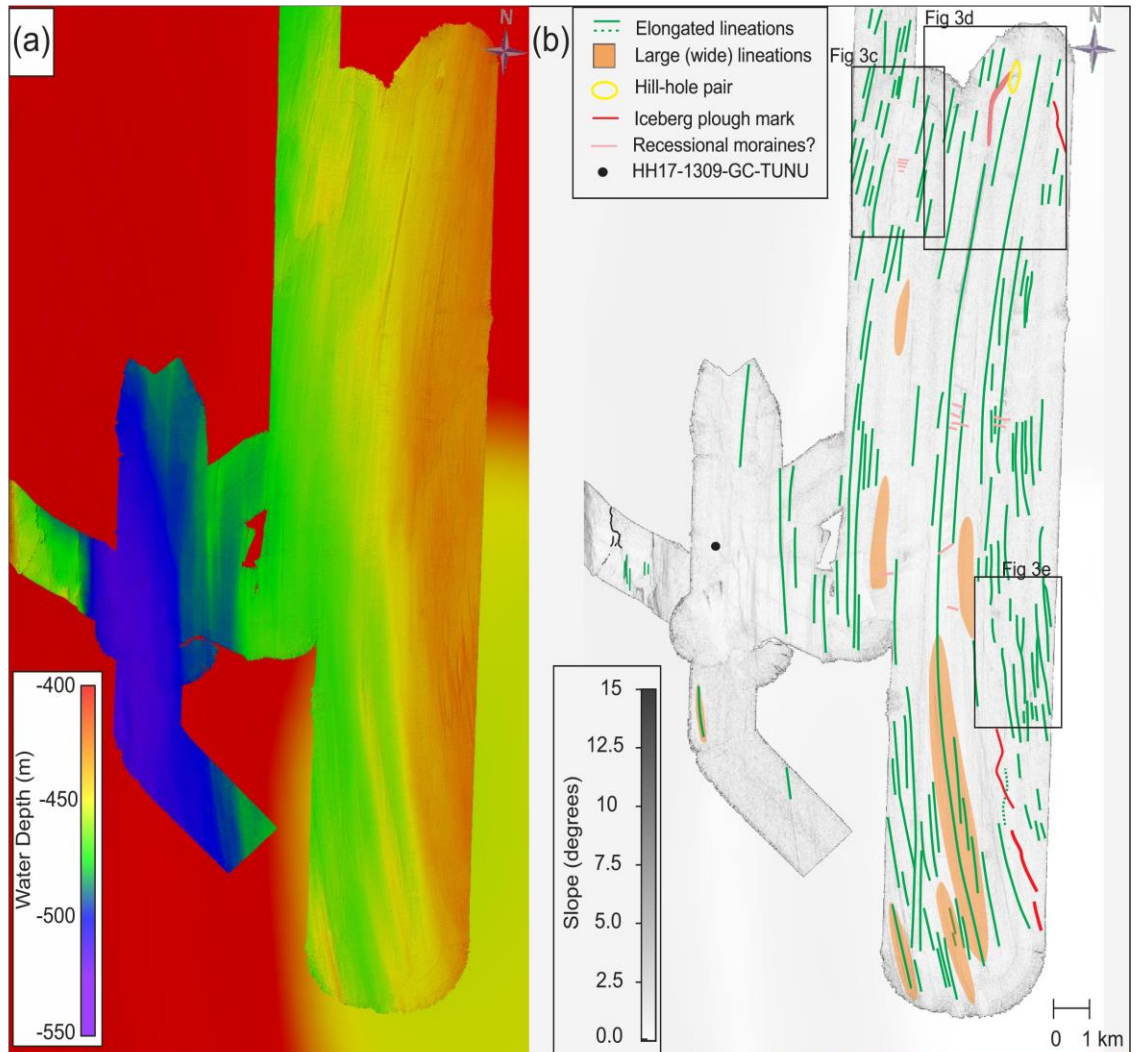
370

371

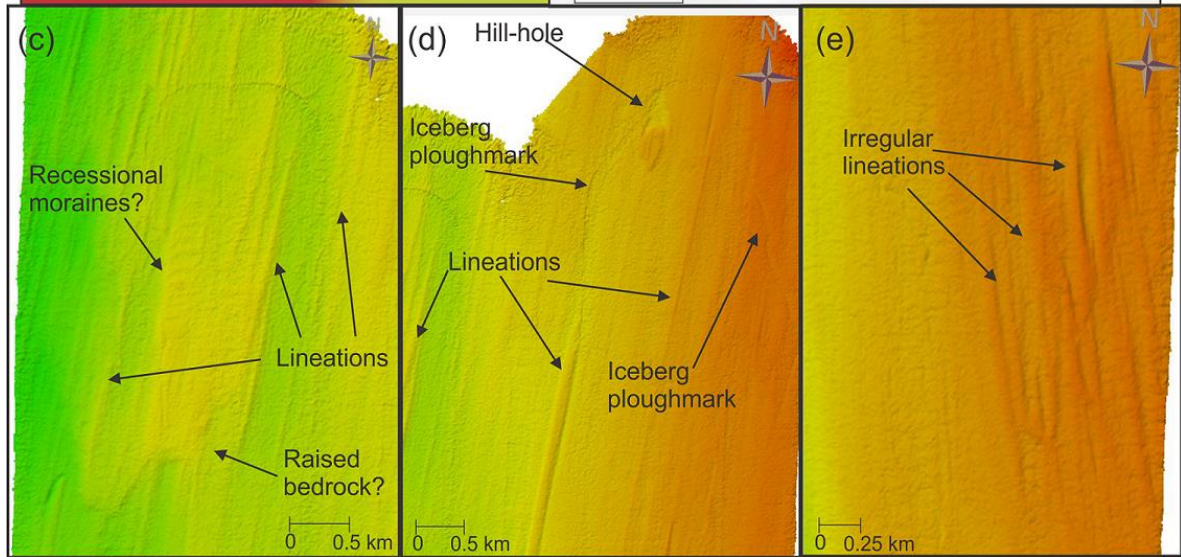
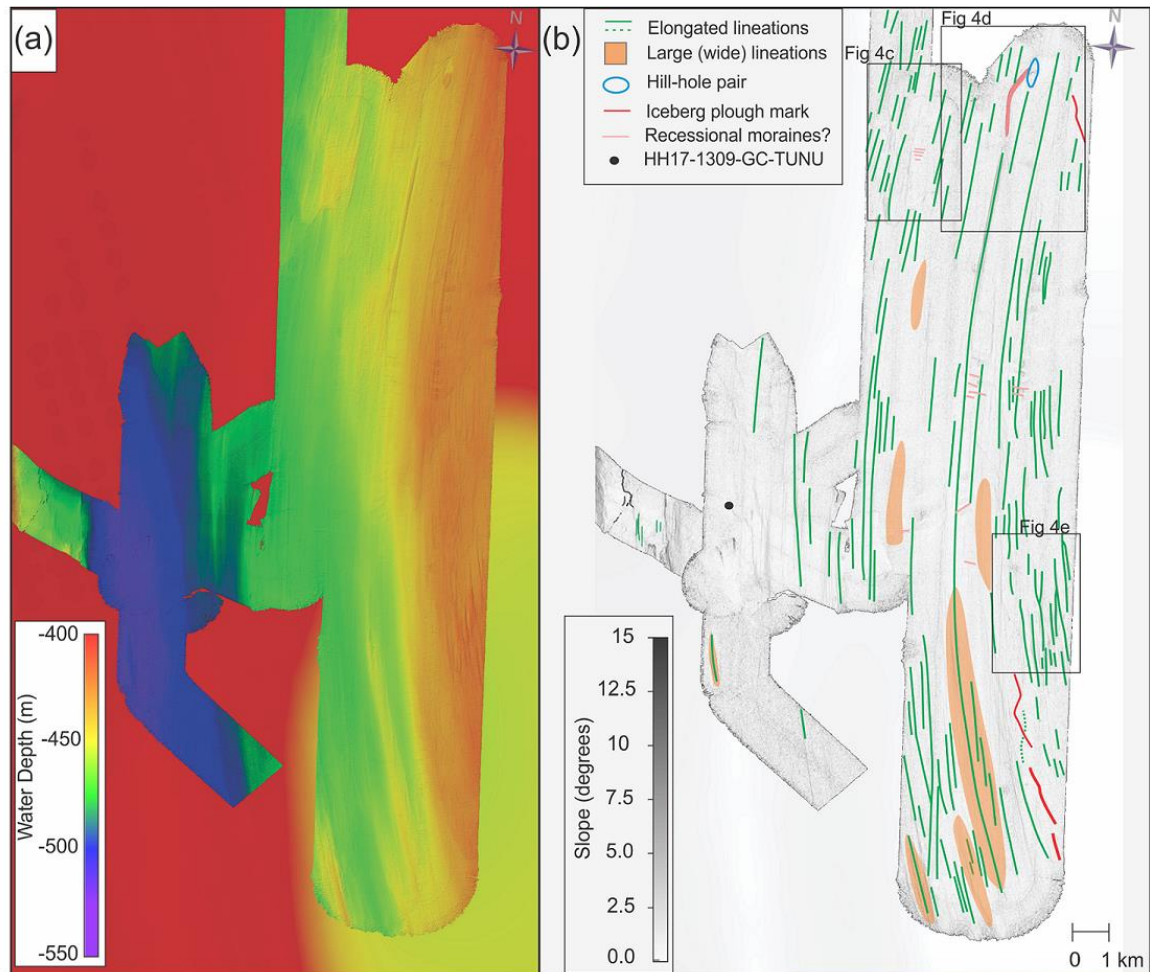
*Table 3. Other published radiocarbon dates and their recalibrated ages using Marine20 (and an ΔR of -10 ± 60) in conformity with (Jackson et al. (2022)) and IntCal20 for aquatic moss samples. *The age of sample Lu-1298 from Shannon is above what is recommended by (Heaton et al., (2022)) for use with Marine20 and is therefore treated with caution.*

Location	Material	Lab nr.	^{14}C age	^{14}C cal BP (1 σ range)	^{14}C cal BP (median)	Reference
Shannon	shell	Lu-1298*	19000 \pm 190	21855-22325	22078	Hjort, 1981; Hjort 1979
Hochstetter F.	shell	Lu-1289	9190 \pm 90	9572-9926	9779	Hjort, 1981; Hjort 1979
Shannon	shell	Lu-1389	9370 \pm 90	9865-10195	10015	Hjort, 1981; Hjort 1979
Hochstetter F.	shell	Lu-1386	9400 \pm 90	9896-10220	10054	Hjort, 1981; Hjort 1979
Hochstetter F.	shell	Lu-1300:1	9470 \pm 90	9970-10322	10157	Hjort, 1981; Hjort 1979
Hochstetter F.	shell	Lu-1300:2	9520 \pm 90	10084-10412	10229	Hjort, 1981; Hjort 1979
Hochstetter F.	shell	Lu-1384	9810 \pm 95	10409-10794	10617	Hjort, 1981; Hjort 1979
Ardencaple Fjord	shell	Lu-1390	8570 \pm 85	8864-9200	9022	Hjort, 1981; Hjort 1979
Kildedalen	shell	Lu-1303	8930 \pm 90	9290-9573	9447	Hjort, 1981; Hjort 1979
Snenæs	Mya truncata,	T-9372	8265 \pm 95	8434-8768	8619	Landvik 1994
	Hiatella arctica					
Hvalrosodden moraine	Nuculana	TUa-123	8685 \pm 95	9006-9315	9166	Landvik 1994
	pernula					
Hvalrosodden moraine	Nuculana	TUa-124	9045 \pm 90	9438-9741	9596	Landvik 1994
Hvalrosodden	Mya truncata	T-9361	8190 \pm 95	8360-8663	8523	Landvik 1994
Hvalrosodden	Mya truncata,	T-9370	7930 \pm 120	8681-9085	8890	Landvik 1994
	Hiatella arctica					
Hvalrosodden	Mya truncata	T-9371	7490 \pm 115	8186-8502	8348	Landvik 1994
Peters Bugt	Portlandia	Ua-2787	10260 \pm 105	11071-11444	11253	Björck, 1994
	arctica					
Peters Bugt Sø	Hiatella arctica	Lu-3516	9640 \pm 90	10222-10527	10382	Björck, 1994
Storstrømmen Sound	Mya truncata &	K-6098	5180 \pm 95	5220-5520	5352	Weidick et al., 1994
	Hiatella arctica					
Storstrømmen Sound	Mya truncata	K-5494	4910 \pm 85	4865-5175	5028	Weidick et al., 1994
Storstrømmen Sound	Mya truncata	K-5493	4840 \pm 90	4793-5117	4943	Weidick et al., 1994
Storstrømmen Sound	Hiatella arctica	Ua-3347	5030 \pm 75	5023-5311	5166	Weidick et al., 1994
Storstrømmen Sound	Hiatella arctica	Ua-3350	4180 \pm 60	3944-4225	4082	Weidick et al., 1994
Storstrømmen Sound	Balanoptera	K-6096	3630 \pm 90	3230-3530	3380	Weidick et al., 1994
	physalus					
Storstrømmen Sound	Hiatella arctica	Ua_3349	3725 \pm 60	3371-3616	3496	Weidick et al., 1994
Storstrømmen Sound	Hiatella arctica	K-6097	3230 \pm 85	2749-3024	2897	Weidick et al., 1994
	& Mya truncata					
Storstrømmen Sound	Hiatella arctica	Ua-3348	1815 \pm 55	1115-1317	1217	Weidick et al., 1994
Hjort Lake	Warnstorfia	Poz-6194	8260 \pm 50	8456-8722	8602	Wagner, 2008
	exannulata					
Duck Lake	Aquatic moss	LuS-6525	8690 \pm 230	9527-10145	9775	Klug 2009

372



373
 374
 375
 376



377
 378 Figure 4. Bathymetric maps from SW Dove Bugt. (a) Seafloor relative to water depth with IBCAO 4.0 displayed in the
 379 background (Jakobsson et al., 2020). (b) The main landforms and slope angles of the seafloor in SW Dove Bugt.
 380 Locations of Figs. 4c-e are indicated. (c) Bathymetry of the northwestern section of the study area. (d) Bathymetry of
 381 the northeastern part of the study area. (e) Bathymetry of the eastern part of the study area showing irregularly
 382 shaped glacial lineations.

383 ~~identified in clusters overprinting the lineations (Fig. 4c), where furrows have been found cross~~
384 ~~cutting lineations (Fig. 4d). Lateral ridges measure 0.5 to 2 m in height and are spaced~~
385 ~~approximately 45 to 250 m apart from each other.~~

386 These elongated lineations are interpreted as glacial lineations (e.g., Ó Cofaigh, 2005). The
387 thinner, more common lineations (with length/width-ratios >10:1) have been interpreted as
388 mega-scale glacial lineations (MSGL), and such landforms are commonly associated with
389 palaeo-ice stream environments (e.g., Stokes & Clark, 2001). Glacial lineations have been
390 identified in numerous continental shelf regions around Greenland (Evans et al., 2009;
391 Dowdeswell et al., 2014; Slabon et al., 2016; Laberg et al., 2017; Newton et al., 2017; Arndt,
392 2018; Batchelor et al., 2018; Jakobsson et al., 2018). While the mechanism behind the
393 formation of these features are still being debated, some authors have suggested that they may
394 have formed through meltwater flooding (Shaw et al., 2008), groove-ploughing (Clark et al.,
395 2003) or the transverse flow in basal ice (Schoof and Clarke, 2008). King et al. (2009), who
396 viewed the formation of MSGL in real time in West Antarctica favored aspects of the dilatant till
397 instability model, but with till properties that could explain ribbed moraine formation and the
398 development of these landforms on a decadal timescale. Sets of ridges that overprint the glacial
399 lineations have been interpreted as recessional moraines, where furrows have been interpreted
400 as iceberg plough marks.

401 *4.1.2. Depression and Mound- Hill-Hole Pair*

402 In northern Store Bælt, a 200 by 450 m wide, 3-4 m deep depression has been identified next to
403 a mound with a width and height of 235 by 450 m and 3-4 m, respectively (Fig. 4d). The
404 depression overprints N-S trending lineations, although the mound contains lineations on its
405 surface.

406 This depression and mound have been interpreted as a hill-hole pair. These landforms can form
407 when ice-thrust rafts of sediment are removed from the bed by cold-based, slow-flowing ice that
408 transports the sediment that was once in the depression (Hogan et al., 2010; Klages et al.,
409 2013, 2015). In this instance, a south bound ice stream may have removed frozen sedimentary
410 material and deposited it further south.

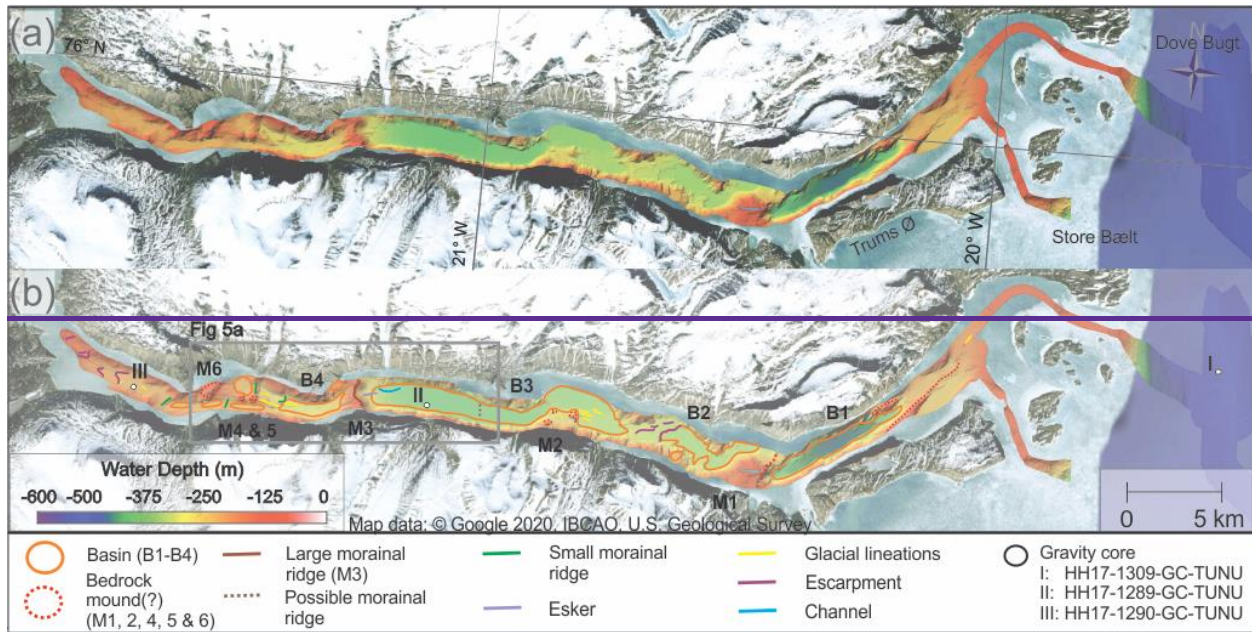
411 *4.2. Sea floor landforms in Bessel Fjord*

412 *4.2.1. Large scale geomorphology*

413 Bessel Fjord contains a variety of basins that are separated by different styles of sills (Figs. 2, 5
414 & 6). The outermost sill is at the fjord's entrance, and it commonly ranges in depth from 50 to
415 200 m, with major sections reaching above (and near) the water surface as there are islands in
416 the fjord entrance. Four large basins that are elongated in a west-east direction have been
417 identified in Bessel Fjord (B1-B4). The deepest basin, Basin 1 (B1), is the closest to the fjord
418 entrance and is separated from basin 2 (B2) by a >215 m high sill (M1) that is steeper to the
419 east (Figs. 2 & 5). Basin 3 progressively deepens westwards, with a maximum depth of 380 m.
420 A ~70 to 160 m asymmetrical sill (M3; Figs. 2 & 5) that is steeper on its east side separates
421 Basin 3 from basin 4. Basin 4 is the shallowest basin (~280-300 m) and is adjacent to multiple
422 smaller basins that are primarily at lower points of elevation. The fjord also contains smaller
423 basins that are raised relative to the average seafloor depth (Fig. 6e). Features interpreted as
424 bedrock mounds have also been identified in other sections of the fjord (Figs. 5 & 6). Along the
425 fjord sides, landforms from sediment reworking including slide scars, channels and gullies have
426 also been observed Fig 6b.

427 **4.2.2. Linear Ridges Oriented Along Fjord Axis- Glacial Lineations**

428 Oriented along the fjord's axis (or at times slightly oblique to it), linear features have been
 429 identified in the inner and middle of the fjord, as well as a single lineation on the outer part of the
 430 fjord (Figs. 5 & 6). They range in size from 100 to 1000 m in length and ~3 to 9 m in height,
 431 although some that are as high as 80 m have been identified in the inner fjord. Their
 432 morphologies vary throughout the fjord, and their length to width ratios range from 2:1 to 5:1.
 433 Most ridges slope towards the outer fjord, although some slope in the opposite direction or have
 434 an irregular or flat top. They appear both independently in connection with inferred bedrock
 435 highs, and in clusters in flat lying areas of basin 3. These ridges have been interpreted as
 436 glacial lineations, and they are thus indicating the direction of former glacier flow.



438 **Figure 5. (a) Bathymetric map of Bessel Fjord. (b) A map of mapped features in Bessel Fjord.**
 439 **Satellite images obtained from Google Earth (© Google 2020).**

450
451

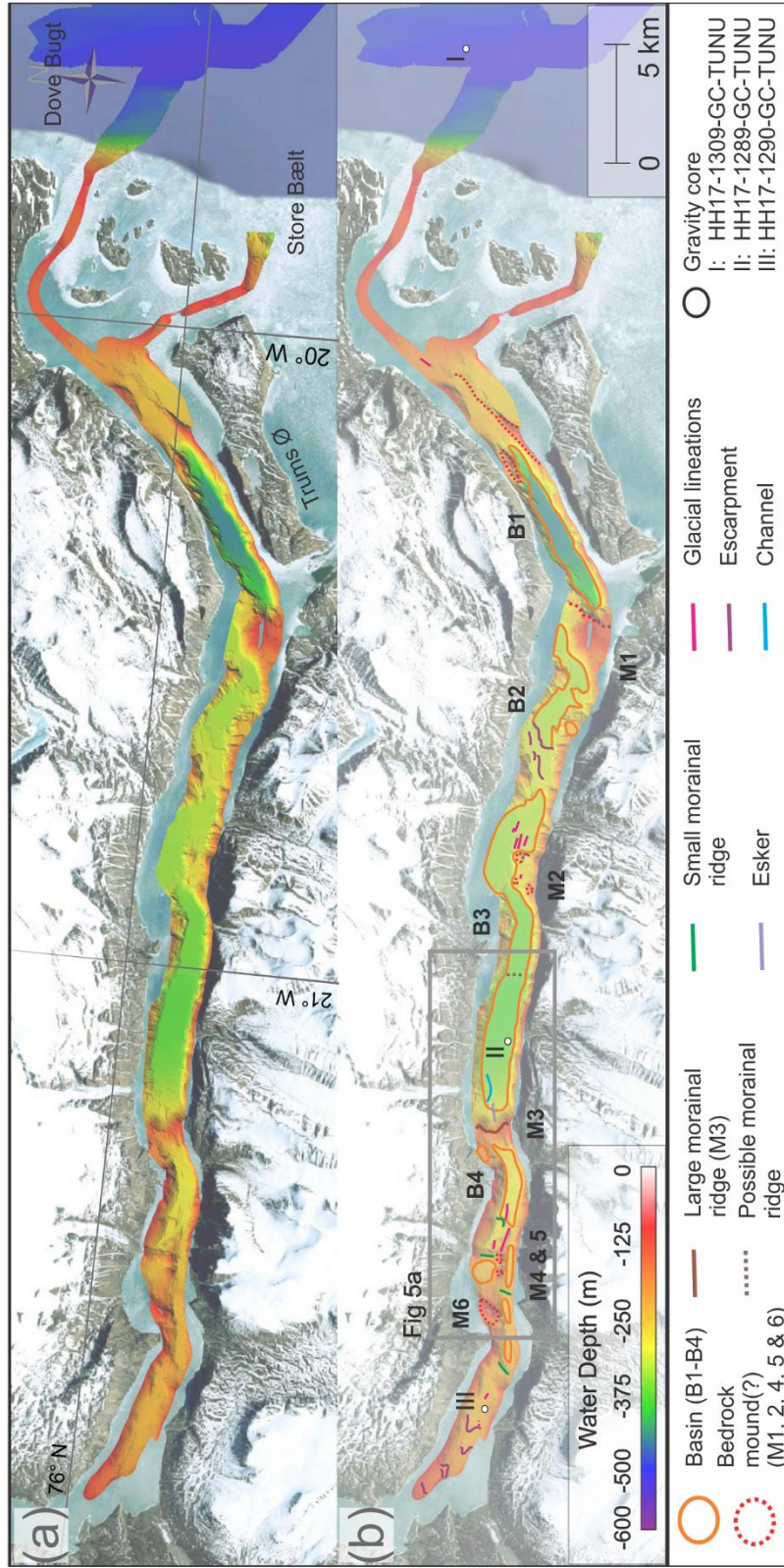


Figure 5. (a) Bathymetric map of Bessel Fjord. (b) A map of mapped features in Bessel Fjord. Satellite images obtained from Google Earth © Google 2020.

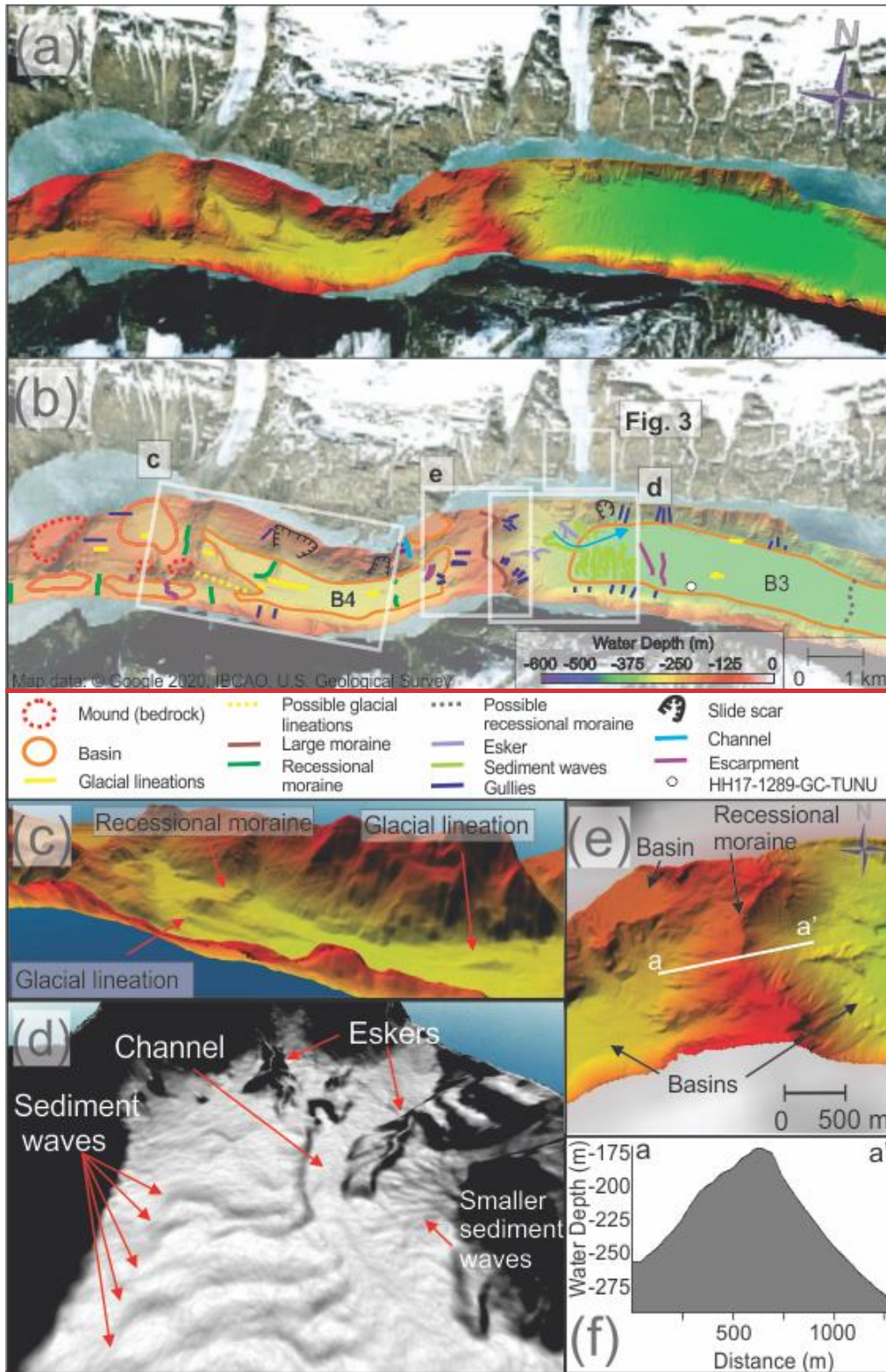
452 *4.2.3. Transverse Ridges- Moraines*

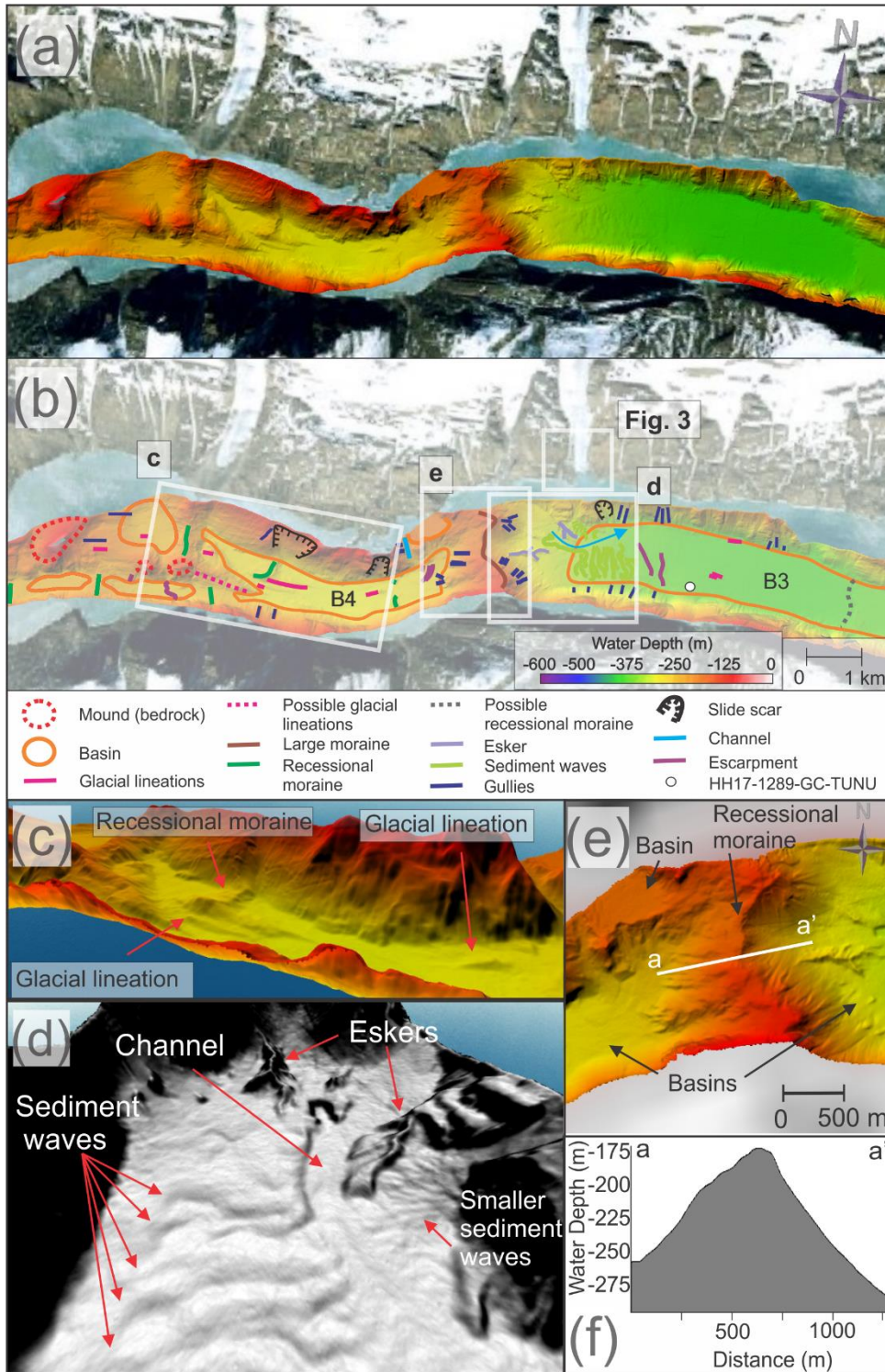
453 Several transverse ridges have been identified in the inner and central portion of the fjord,
454 oriented perpendicular to the fjord's axis (Figs. 2, 5 & 6). The ridges in the inner most position of
455 the fjord tend to largely conform to the topography (~~i.e.~~, between bedrock mounds, some of
456 which are position mid-fjord (M4-6; Fig. 6b), and the fjord sidewalls) and are ~~, at times,~~ the
457 threshold between sub-basins (Fig. 6). The width and length of ridges range from 150 to 600 m
458 and 120 to 500 m, respectively, where their heights are between <5 to 58 m.

459 A particularly large, asymmetrical transverse ridge that spans the width of the fjord, is situated
460 between Basin 3 and 4 (M3; Figs. 2 & 6d). This ridge is ~1.5 km in width and between 72 to 162
461 m in height. It contains a crescent shape in aerial view and is concave towards the mouth of the
462 fjord. A large threshold with a 1.8 km width and a > 215 m height also separates basin 1 and 2
463 (M1; Figs. 2 & 5). This feature is ~150m shallower in the north and dips steeply into basin 1.

464 The transverse ridges have been ~~interpretation~~ interpreted as moraines, which would have
465 formed during glacial stillstands or readvancements during the retreat of a grounded tidewater
466 glaciers margin. These moraines do not fill the width of the innermost fjord, which has also been
467 seen in inner Nordfjord (part of the Keiser Franz Josef fjord system) by Olsen et al. (2022).

468 While the large transverse ridge M3 is believed to be a moraine, it is considered more likely that
469 M1 is a bedrock mound based on its morphology. The smaller transverse ridges are interpreted
470 as recessional moraines. Smaller moraines have the potential to form at ice margins annually
471 (Lyså & Vorren, 1997; Dowdeswell et al., 2016) and have been observed with a variety of sizes
472 and morphologies on the NE Greenland shelf (e.g., Winkelmann et al., 2010).





476

477 Figure 6. (a-b) Mapped sections from inner to middle Bessel Fjord. (b) *Glacial lineations in Basin 4 (B4)*. Background
 478 images used for 6a & 6b obtained from Google Earth (© Google 2020). (c) *Glacial lineations in Basin 4 (B4)*. (de)
 479 Eskers, sediment waves and a channel in Basin 3 (B3). (ee) A large moraine (M3) between B3 and B4. Note the
 480 raised sub-basin to the west and esker to the east. (fe) Profile across the large recession moraine (M3).

4.2.4. Sinuous Ridges- Eskers

481 Sinuous ridges, oriented parallel or oblique to the fjord's axis, occur in basin 3 (Figs. 5, 6b, 6d
482 &6e). These features have widths and lengths of 50 to 120 m, 350 to 800 m, respectively and
483 heights of 10 to 15 m. The most pronounced examples of these ridges have been observed east
484 of the large recessional moraine that has been previously discussed (Fig. 6e).
485

486 These sinuous ridges have been interpreted as eskers. These landforms form from sediment
487 infill of subglacial and englacial conduits ~~and have been identified in other studies in Greenland~~
488 (Huddart and Lister, 1981; Geirsdóttir et al., 2000; Winkelmann et al., 2010; Lane et al., 2015).
489 They frequently form in the direction of former ice flow and often form during terminal stages of
490 glaciation, and are therefore associated with moraines (Shreve, 1985). They vary in size
491 depending on the glacial drainage pattern, as well as a number of other factors, however eskers
492 identified within Bessel Fjord appear smaller than those identified in studies in Canada, the UK
493 and Kola Peninsula in Russia (Storrar et al., 2014)

4.2.5. Wavy Transverse Ridges- Sediment Waves

494 Adjacent to the two eskers in Basin 3 are a series of wavy transverse ridges to the east of a
495 large recessional moraine (Figs. 5, 6b & 6d). These features occupy an area of ~500 by 1500 m
496 and contain small ridges and flat areas that slope at an angle of 3 to 6° to the east. Each wave
497 "crest" is ~50 to 100 m apart, although some appear to begin only halfway through the width of
498 the area, where others occupy the entire width, north to south. These waves are crosscut by a
499 channel to the north (Fig. 6d). North of this channel similar features with a wavy morphology
500 occur, although these are substantially smaller.
501

502 These wavy transverse ridges have been interpreted as sediment waves. Sediment waves
503 found associated with deltaic and glacialfluvial deltaic systems have been associated with
504 retrogressive slope failures, gravity-induced sediment creep and/or the migration of sediment
505 waves upslope (Cartigny et al., 2011; Hill, 2012; Stacey and Hill, 2016). Alternatively, given the
506 position of the smaller wavy transverse ridges to the ice cap on Ad. S. Jensen Land (Figs. 1 &
507 2) and the larger ridges to the large moraine to the west (Figs. 5 & 6) it is also possible that
508 these ridges are sets of moraines. Recessional moraines have been identified in the vicinity of
509 eskers in Spitsbergen fjords (Ottesen et al., 2008; Kempf et al., 2013), which may account for
510 the ~~small or~~ wavy transverse ridges. The larger wavy transverse ridge do also resemble
511 thrust moraines identified by Forwick et al. (2010). Further work may be required in the
512 evaluation of these features. ~~for~~ or a full list of observed landforms see Table 4.

4.3. Lithostratigraphy

513 Three gravity cores were retrieved from the study area. Gravity core HH17-1309 was collected
514 in ~~western Store Bælt, just outside of Bessel Fjord. This core has~~ and was sampled from a
515 N/NW-S/SE oriented depression that contains iceberg ploughmarks and a MSGL ~~and includes~~
516 lithological units of mud and a diamict (Figs. 7a-e). Gravity core HH17-1289 was collected in the
517 middle of the Bessel Fjord ~~and, near the southern sidewall of the fjord. The core~~ is located
518 directly east of the above-mentioned sediment waves on the distal part of the pronounced
519 transverse ridge. Nearby, a modern ice cap fed glacialfluvial channel is observed in satellite
520 imagery, likely with a delta at its fjord termination. ~~This core contains a substantially higher sand~~
521 ~~content than other cores collected in the region (Units 2.2-2.4).~~ The gravity core HH17-1290,
522 ~~comprising mostly muddy deposits (Units 3.1-3.3),~~ was collected within the inner fjord. ~~The~~
523 ~~gravity core is~~ west of the basins and thresholds observed in this study area, and is the closest
524 core to Soranerbræen (located ~~about~~ ~9.7 km east of the glacier) (Fig. 7).
525

527 *Table 4. Overview of observed landforms in southern Dove Bugt and Bessel Fjord.*

Region	Description	Width	Length	Height	Notable Feature	Interpretation
Dove Bugt	Elongated lineations	35-50 m	~1->10 km	<1-3 m	Roughly N-S	Glacial Lineations
	*Wide	200-650 m	3.8 to 8.8. km	4.5-15 m		
	Depression and mound	200 m	450 m	3-4 m	Mound to the south of the depression	Hill-hole pair
	Furrows (scour marks)	~40-100 m	<100-200	3-5 m	Irregular	Iceberg plough marks
	Transverse ridges	150-400 m	~30-100 m	0.5-1 m	Roughly W-E	Recessional moraines
Bessel Fjord	Linear ridge	45-350 m	100-1000 m	3-9, 80 m	Parallel to the fjords axis	Glacial Lineations
	Transverse ridges	150-600 m	120- 500 m	<5-58 m	Perpendicular to the fjords axis	Recessional moraines
	*Large ridge (M3)	1485 m	600-1600 m	72 to 162 m		Moraine
	Sinuuous ridges	50-120 m	350-800 m	10-15 m		Esker
	Wavy transverse ridges	400-700 m	~45-100 m	2-5 m	Perpendicular to the fjords axis	Sediment wave
	Elongated depression	~200 m	~1 km	6-8 m		Channels
	Chute	~20-100 m	60-400 m	1-15 m		Gullies

528

529

4.3.1. Facies

530

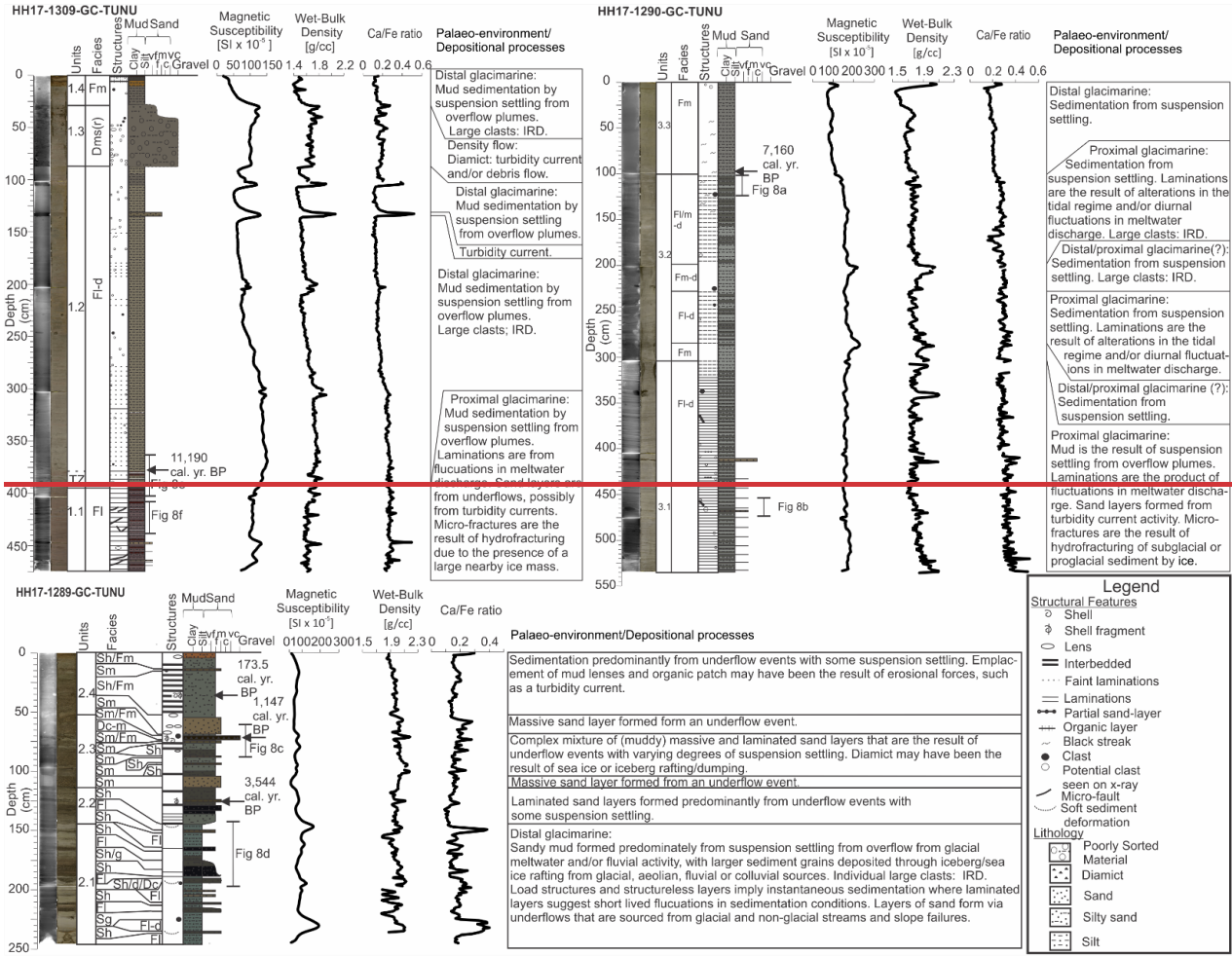
Facies 1 – Laminated Mud (Fl, Fl-d & Fl/m-d)

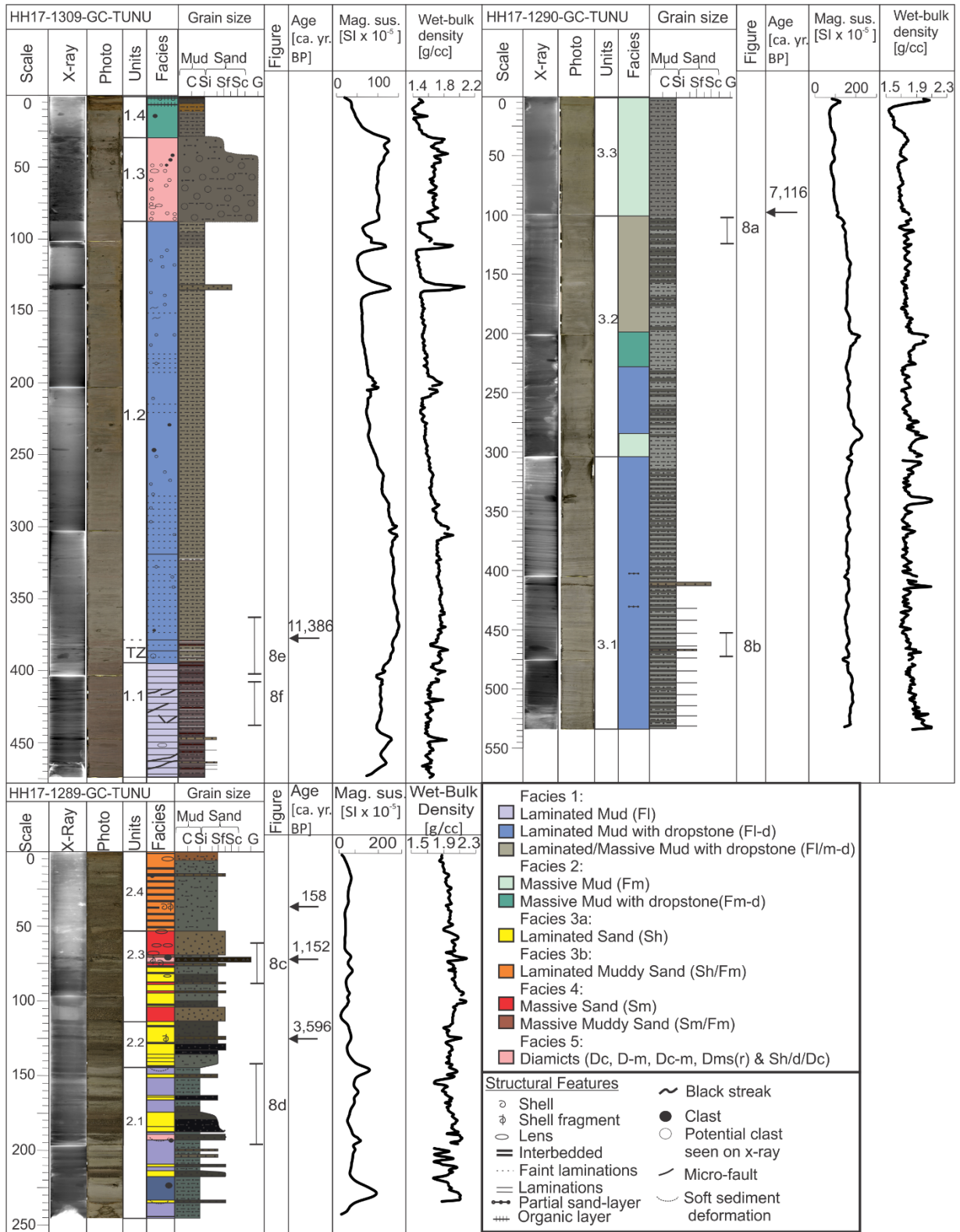
531 Facies 1 consists of laminated mud (Fl) and laminated mud with dropstones (Fl-d) and have
532 been observed in all three gravity cores (Figs. 7, 8a, 8d & 8f)). Laminations are composed of
533 either mud or very fine sand. Mud laminations with finer laminations have also been identified in
534 Unit 3.2 (100-200 cm; Fig. 7a, Fl/m-d). Microfractures have also been identified within this facies
535 (Fig. 8f).

536 Wet-bulk density measurements tend to increase with depth in some sections of this facies
537 (e.g.e.g., 87-350 cm in HH17-1309), suggesting normal sediment consolidation. However, a
538 stagnation or decrease in wet-bulk density with depth in other sections (e.g.e.g., below ~350 cm
539 in HH17-1309) suggests less ~~or no~~ consolidation. The magnetic susceptibility generally tends to
540 increase with depth in HH17-1309 and in Unit 3.2 in HH17-1290, however the remainder of this
541 facies in HH17-1290 (Unit 3.1) remains relatively stable to the base of the core. Notable positive
542 peaks have been identified at 110 and 140 cm in HH17-1309 and measurement fluctuations
543 occur in HH17-1289. Peaks in magnetic susceptibility may reflect the introduction of turbidites or
544 clasts where fluctuations may reflect shifts in sediment provenance.

545 Muds with sand laminations are believed to have formed through a combination of ice-proximal
546 suspension settling from overflow plumes and turbidity-current activity (underflows). The
547 rhythmically laminated muds are believed to have formed from ice-proximal suspension settling
548 from turbid overflow plumes. Similar laminated sediments have been identified in Kejser Franz

549 Joseph Fjord and Fosters Bugt in East Greenland and are theorized to have been deposited
550 from turbid meltwater plumes in an ice-proximal environment (Evans et al., 2002) by (Cowan et
551 al., 1999; Forwick and Vorren, 2009) ~~in Svalbard~~. Large clasts have been interpreted as ice
552 rafted debris (IRD) and the formation of microfractures may have been caused by soft
553 sediment deformation, possibly from grounded icebergs, possibly including hydrofracturing, from
554 subglacial or proglacial processes. Similar soft, marine sediment deformation from a glacial
555 environment has previously discussed by Passchier (2000) in Antarctica.





557

558

559

560

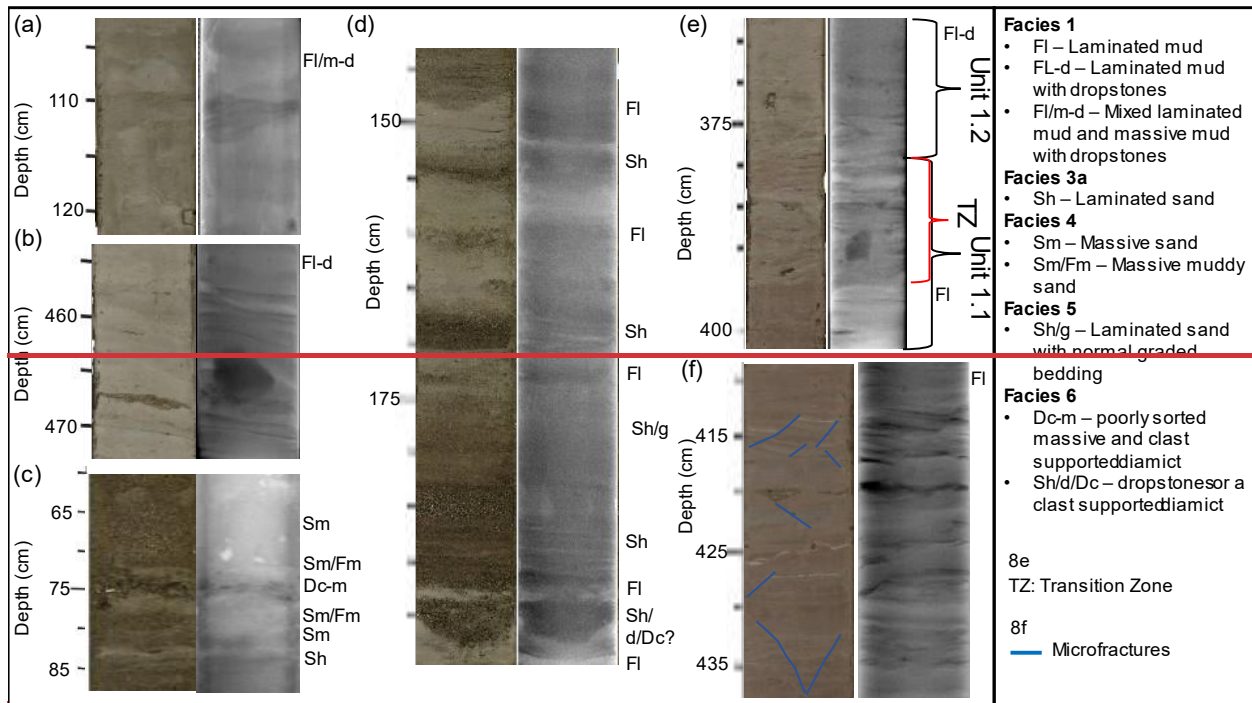
561

Figure 7. Lithological core logs of the three gravity cores with x-ray images, core photos, unit divisions, facies, structures, magnetic susceptibility and wet-bulk density. TZ in HH17-1309-GC-TUNU stands for "Transition Zone". Grain size abbreviations: C: clay, Si: silt, Sf: fine grained sand, Sc: coarse grained sand and G: gravel.

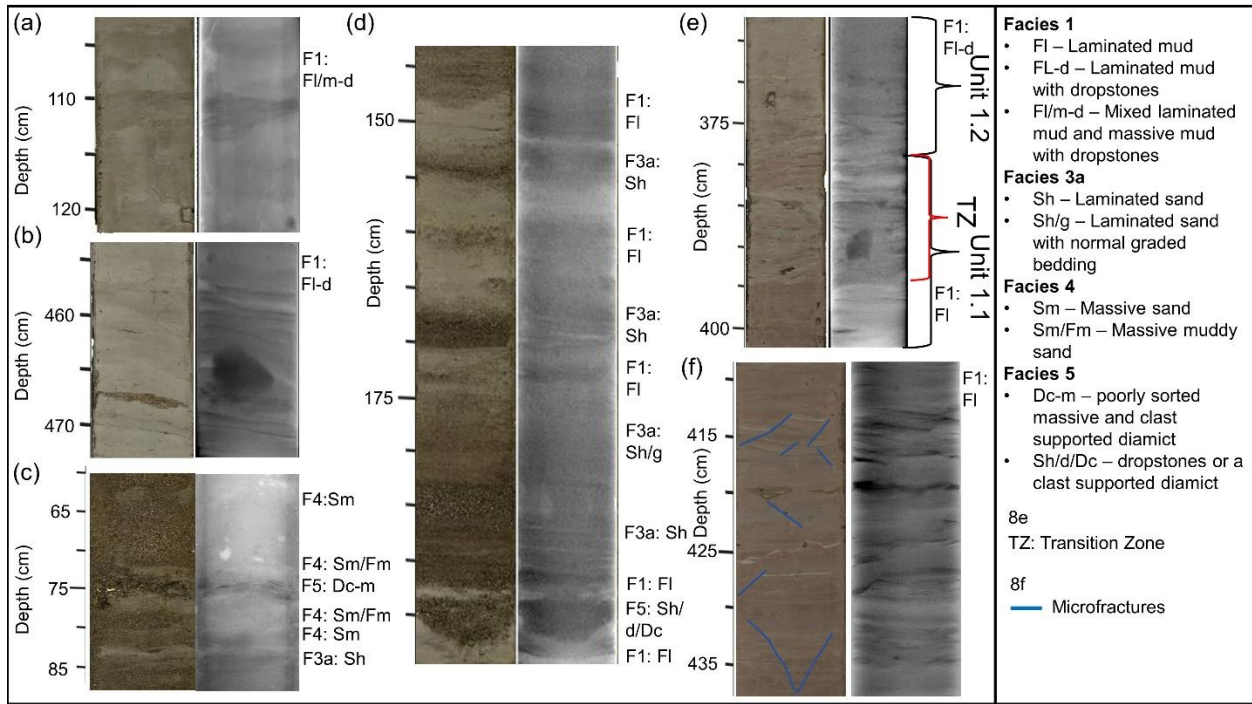
562 *Facies 2 – Massive Mud (Fm & Fm-d)*

563 The second facies consists of massive mud with or without dropstones and can be found in the
564 inner fjord core HH17-1290 and the Store Baelt core HH17-1309 (Fig. 7). In HH17-1290 this
565 appears downcore between sections of Facies 1 as well as in the topmost unit, Unit 3.3. The
566 magnetic susceptibility gradually increases downcore in this facies in Unit 3.3. Further down
567 core, in Unit 3.2, this facies is associated with a downwards trend in magnetic susceptibility
568 following peaks in measured readings. Wet bulk density values roughly mirror these trends. In
569 HH17-1309 massive mud units have been observed in Unit 1.4, where magnetic susceptibility
570 and wet bulk density values increase downcore.

571 This facies is interpreted as being the result of suspension settling from overflow plumes and is
572 believed to have been deposited in an ice-distal glacial marine environment with varying input from
573 IRD (i.e., Boulton & Deynoux, 1981). Sediment may be sourced from a single location (i.e.,
574 Soranerbræen) or more than one location (e.g.e.g., local ice caps) in an ice-distal glacial marine
575 environment with limited iceberg or sea-ice rafting. Massive mud deposits have also been
576 identified in other Greenland fjords (e.g., Ó Cofaigh et al., 2001) and it has been suggested that
577 they may indicate meltwater from ice- or fjord margin-distal conditions (Evans et al., 2002).



578



579

580 *Figure 8. Photographic and x-ray images of sections of the three gravity cores (a-f). Corresponding facies codes can*
 581 *be found to the right of each image.*

582 **Facies 3a – Laminated Sand (Sh)**

583 Facies 3a consists of sections of sand with horizontal sand laminations. This facies has been
 584 predominantly observed in the mid-fjord core, HH17-1289-GC-TUNU (Figs. 7 & 8d). These
 585 sections consist of fine to medium grained sand that range in thickness and colors. Occasionally
 586 this facies also contains normal graded bedding (e.g., Fig. 8d, ~174-183 cm). This facies does

587 not contain uniform magnetic susceptibility or wet-bulk density readings as it has been found in
588 association with low and high peaks of both parameters as well as values that are near the
589 average for the core.

590 This facies is interpreted as being deposited from turbidity currents, possibly underflows that are
591 either sourced from glacial or non-glacial streams and slope failures. Uniform layers may
592 indicate a single, rapid event, where shifts in grain size and color may be the result of short-lived
593 fluctuations in sediment input. Laminated sands have been identified in Scoresby Sund in East
594 Greenland and have also been attributed to turbidite formation (Ó Cofaigh et al., 2001).

595 *Facies 3b – Laminated Muddy Sand (Sh/Fm)*

596 Facies 3b represents sections of sand with faint horizontal laminations as well as a large
597 quantity of clay material interspersed throughout with faint laminations. This has been observed
598 in HH17-1289 at the topmost unit in the core, Unit 2.4 (Fig. 7). Magnetic susceptibility is
599 relatively uniform in this facies, where the wet-bulk density tends to decrease up core. Sediment
600 grain size analysis of a single sample from this facies revealed that the sediment is composed
601 of 56.3% sand and 43.7% mud. A “patch” of black organic material (*i.e.*, plant material and
602 shells) was also identified within this unit.

603 This complex facies is believed to have formed predominantly from underflow events, sandy –
604 muddy turbidites, alternatively sandy turbidites with additional input from suspension settling.
605 Similar deposits have been observed in Balsfjord, Norway although without lamination and
606 possibly a higher mud content (Forwick and Vorren, 1998).

607 *Facies 4 – Massive Sand / Massive Muddy Sand (Sm & Sm/Fm)*

608 Facies 4 contains sections of massive sand (Sm) as well as massive sand with a large amount
609 of clay content (Sm/Fm). This facies is predominantly found in Unit 2.3 (and to a much less
610 extent, Unit 2.4) in HH17-1289 (Fig. 7). Sections of massive sand have been found in
611 association with mud lenses and often contain horizontal sand layers (Sh) above and below it.
612 Slight increases and decreases in magnetic susceptibility values have been observed within this
613 facies.

614 This facies is believed to have developed through rapid deposition as well as deformation of
615 Facies 3a & b. According to this interpretation, the mud lenses observed in this facies were
616 once layers/lamina that became deformed due to the sand – mud density contrast. Massive
617 sand has been found in Kangerlussuaq and Miki Fjords in East Greenland (Smith and Andrews,
618 2000) and well-sorted coarse grain deposits have been recovered near Petermann Glacier in
619 northern Greenland (Reilly et al., 2019). Authors have attributed these layers to sediment gravity
620 flows. Massive sand deposits with similar characteristics have also been observed in an
621 Alaskan fjord near Muir Glacier (Cowan et al., 1999).

622 *Facies 5 – Sand with Normal Graded Bedding (Sg & Sh/g)*

623 ~~Facies 5 is used to depict sediment that contains normal graded bedding (Sg) or appear to have
624 clear horizontal laminations and have normal graded bedding (Sh/g). This has been observed
625 in layers of sediment within Unit 2.1 of HH17-1289 (Figs. 7 & 8d). As normal graded sands have
626 been observed in the A layer of the Bouma sequence, it is possible that these layers formed
627 from turbidity currents during underflow events.~~

628 *Facies 56 – Diamicts (Dc, D-m, Dc-m, Dms(r) & Sh/d/Dc)*
 629 Facies 6 contains a variety of different diamicts observed within the mid-fjord core HH17-1289
 630 and the Store Baelt core HH17-1309. In HH17-1289 this includes a 3.5 cm poorly sorted
 631 massive and clast supported diamict (Dc-m) in the middle of Unit 2.3 (Figs. 7 & 8c), and a
 632 horizontally laminated layer of sand that that is either accompanied by dropstones or a clast
 633 supported diamict (Sh/d/Dc) (Figs. 7 & 8d). It is inferred that they are the result of sea ice or
 634 iceberg rafting/dumping. Within HH17-1309 there is a substantially larger, sharp based, matrix-
 635 supported diamict, stratified in its upper part (Dms(r)) in Unit 1.3 (Fig. 7). Based on these
 636 characteristics, this diamict has been interpreted as a density flow deposit, likely a debris flow
 637 deposit that is overlain by (part of) a turbidite.

638 4.3.2. Chronology and sedimentation rates

639 Shell and shell fragments were recovered from HH17-1289 for radiocarbon dating. At 34 cm
 640 depth, a semi-spherical path of organic content was identified, containing two intact *Yoldiella*
 641 *lenticula*, a shell fragment and plant material. Additionally, at 71 cm depth, a large 3 cm half of a
 642 *Hiatella arctica* shell was collected for dating, and shell fragments were recovered from a depth
 643 of 125 cm for the same purpose. These shells yielded radiocarbon ages of 1,5874, 1,15247 and
 644 3,59644 cal yr. BP, respectively (Table 5-4).

645 Cores HH17-1290 and HH17-1309 were subsampled for foraminifera material at four positions.
 646 Calcareous benthic species, which were rare, were used for dating and include predominantly
 647 *Melonis barleeanus* as well as *Islandiella norcrossi*, but in substantially smaller quantities. In
 648 HH17-1309, at a depth of 377 cm *Islandiella norcrossi* (rare to common) & *Stainforthia feylingi*
 649 (rare) and a planktonic species were identified immediately above the transition zone between
 650 deformed (below) and undeformed sediments (above). Radiocarbon dates for the HH17-1309
 651 sample yielded an age of 11,386490 cal yr. BP where the sample from HH17-1290 yielded an
 652 age of 7,11660 cal yr. BP (Table 5-4).

653 Table 5. Radiocarbon dates, calibrated dates, and associated linear sedimentation rates.

Coring station	Sampling Depth [cm]	Lab nr.	Species	¹⁴ C age BP	Marine20 cal BP (1σ range)	Marine20 cal BP	Linear sedimentation interval [cm]	Linear sedimentation rate Marine20 [cm/ka]
HH17-1309-GC-TUNU	377	5157.1.1	Mixed benthic foraminifera	10357 ± 95	11201 - 11553	11386	0-377	33.11
HH17-1289-GC-TUNU	35	5154.1.1	<i>Yoldiella lenticula</i>	688 ± 34	61 - 253	158	0-35	221.52
HH17-1289-GC-TUNU	71	5155.1.1	<i>Hiatella arctica</i>	1747 ± 28	1065 - 1250	1152	35-71	31.25
HH17-1289-GC-TUNU	125.5	5156.1.1	Bivalve frag.	3809 ± 36	3472 - 3701	3596	71-125.5	15.16
HH17-1290-GC-TUNU	97	5158.1.1	Mixed benthic foraminifera	6800 ± 80	6990-7250	7116	0-97	13.63

654
 655 Linear sedimentation rates were calculated assuming modern sediments are at the core top as
 656 no overpenetration was recorded during the sampling of these cores and that during the core

657 logging little sediment disturbance was found (Table 5-4). Given the scarcity of biological
658 material in these cores these sedimentation rates act only as a first approximation until a more
659 detailed record can be recovered. Using the available (calibrated) dating results,
660 ~~S~~sedimentation rates of ~15 cm/ka, ~31 cm/ka, & ~~~22204~~ cm/ka were calculated for core HH17-
661 1289 at 71-125.5 cm, 35-71 cm, and 0-35 cm, respectively. These results reveal an increase in
662 the sedimentation rate towards the present. However, as this core includes multiple deposits
663 from turbidity currents (i.e., reworked deposits), linear sedimentation rates in core HH17-1289
664 should be treated with caution. An average, linear rate of ~~~143~~ cm/ka was calculated for the
665 interval of 0-97 cm in core HH17-1290 and an average, linear rate of ~33 cm/ka was also
666 obtained for the large interval of 0-377 cm in core HH17-1309. ~~These~~ The linear rates are
667 lower, up to an order of magnitude, when compared to the Kejser Franz Josef Fjord system
668 ~400 km south of the study area (Olsen et al., 2022). The origin of this observed difference
669 must await further studies.

670

671 4.3.3. Ca/Fe elemental ratios

672 ~~Large scale trends in Ca/Fe elemental ratios in core HH17-1290 in inner Bessel Fjord, and core~~
673 ~~HH17-1309 in the Dove Bugt, are relatively stable showing a slight increasing trend downcore~~
674 ~~(Fig. 7). This differs from the mid-fjord core, HH17-1289, which is more complex and does not~~
675 ~~contain a single trend. The topmost section of HH17-1290 and HH17-1289 do notably contain~~
676 ~~large peaks in Ca/Fe ratios that strongly decrease a few centimeters into each core. Minor~~
677 ~~peaks increase in frequency downcore in HH17-1290 as the presence of laminations increase.~~
678 ~~In HH17-1309, increased values are also observed in larger sand laminations, sand layers and~~
679 ~~diamict near the top of the core. Minor fluctuations occur throughout HH17-1289, often with~~
680 ~~shifts in ratio values occurring between different layers. This may indicate that within these~~
681 ~~cores minor fluctuations may be the result of changes in sediment provenance. This, however,~~
682 ~~is more complicated in HH17-1289, as many of the layers are reworked sediment (turbidites).~~

683 **5. Discussion**

684 **5.1. Ice Sheet advance**

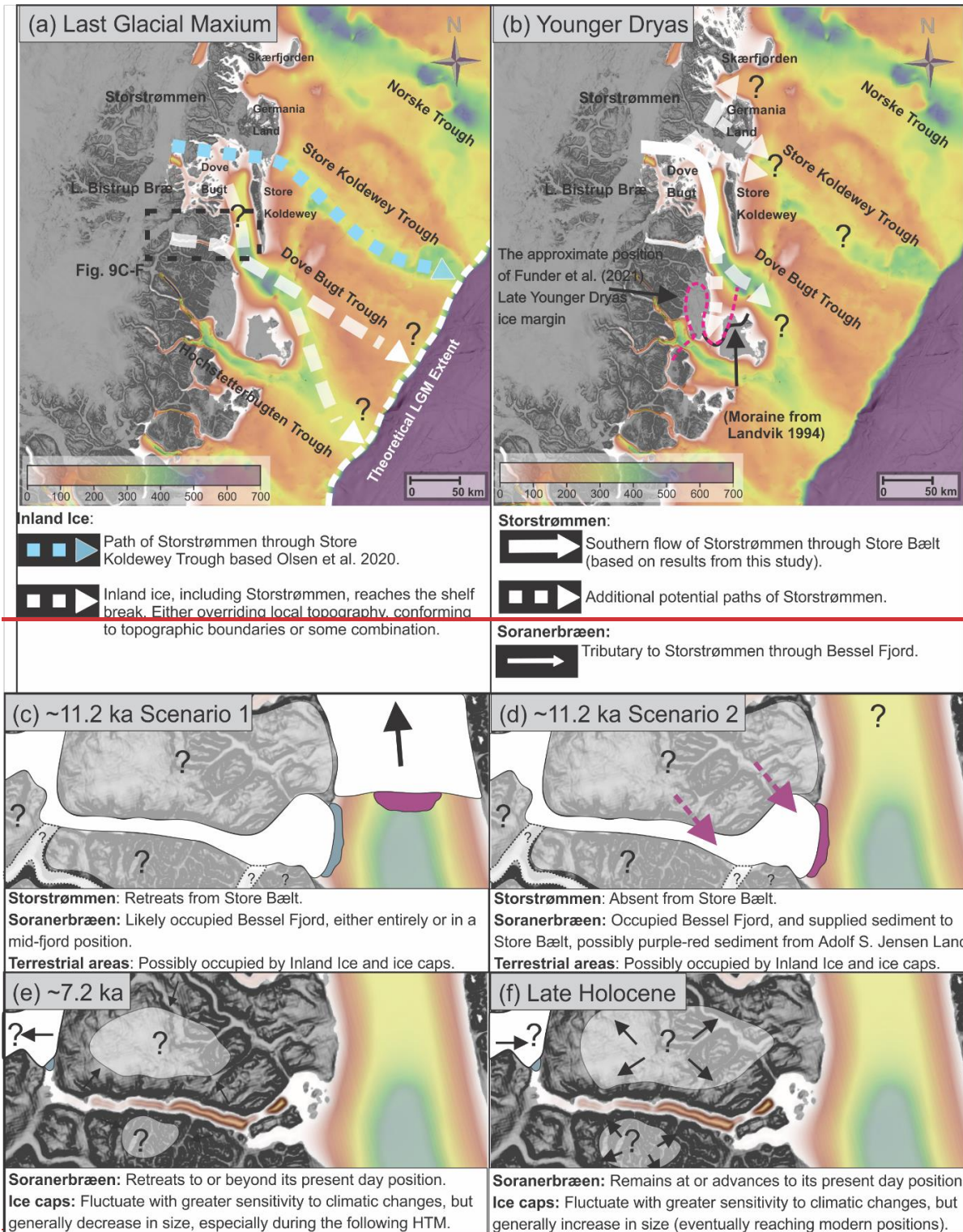
685 The appearance of glacial lineations in Bessel Fjord suggest that the fjord was once fully
686 glaciated, which is in accordance with the inferred shelf break-terminating ice sheet inferred for
687 the LGM from other studies (e.g., Laberg et al., 2017; Olsen et al., 2020) (Figs. 9a & 9b). Ice
688 that filled the fjord is believed to most likely be from the modern Soranerbræen glacier but may
689 have also included ice caps and other nearby branches of inland ice. ~~Additionally, deep basins~~
690 ~~and base-level flattening within the fjord likely originate from multiple (pre-LGM) ice advances~~
691 ~~into the fjord (e.g. Barnes et al., 2016).~~

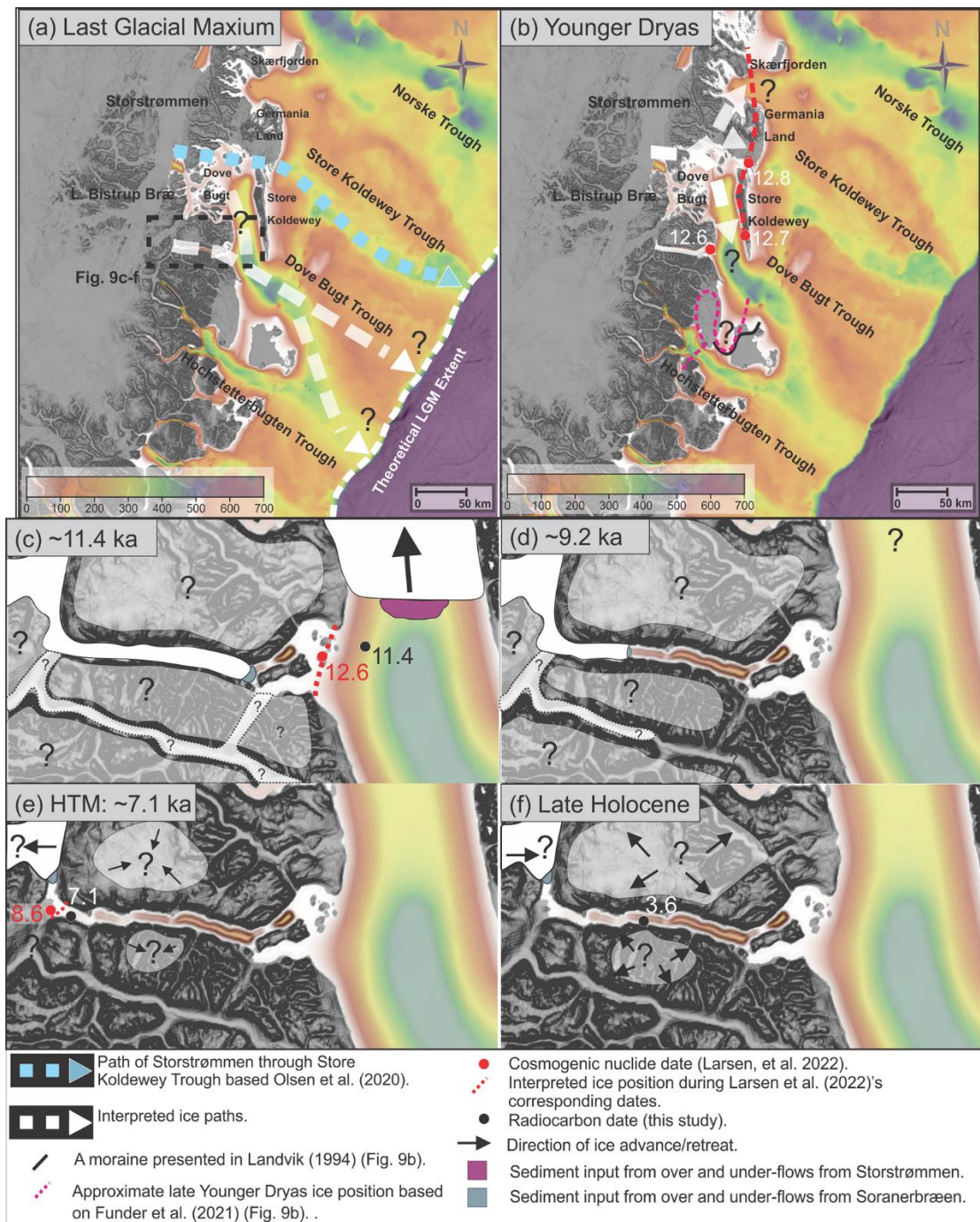
692 Glacial lineations are believed to have formed during the LGM, ~~or~~ but could have also formed
693 during an ice readvance in the deglaciation (see below). Onshore and south of Bessel Fjord,
694 two sets of striations identified in Langsødalen (Hjort, 1979, 1981) may suggest that this valley
695 experienced two glaciation events ~~during this period~~ (Fig. 1c). Striations, and lateral moraines,
696 found along the fjord axis may be the result of the east-west movement of ice through the valley,
697 where SW oriented striations may be the result of Storstrømmen encroaching also onto
698 terrestrial areas. Hjort (1981) suggested that striae on Haystack may indicate that ice flow was
699 dominant from the north during the Nanok Stadial but ice pressure from Langsødalen dominated

700 later after deglaciation begun. Thus, it is possible that ice masses drained through both Bessel
701 Fjord and Langsødalen during full-glacial conditions ~~further-ice Sheet~~ advancing into ~~SW~~ Dove
702 Bugt/Store Bælt.

703 In Store Bælt, the orientation of glacial lineations (~~e.g.e.g.~~, MSGLs) suggest that ice flowed to
704 the south along the west coast of Store Koldewey, marking the southwards expansion of the
705 Storstrømmen ice stream (Fig. 9a & 9b). East of Dove Bugt, MSGLs identified in Store
706 Koldewey Trough are believed to have formed when the Storstrømmen ice stream acted as a
707 “pure” ice stream (Bentley, 1987; Stokes and Clark, 1999) and overrode the underlying
708 topography during the LGM (Fig. 9a; Olsen et al., 2020). It was theorized that at a later phase,
709 when the ice sheet began to thin, the ice stream became more influenced by the topography of
710 deep troughs, draining northwards to Jøkelbugten and southwards to Dove Bugt (Olsen et al.,
711 2020). Assuming these two phases occurred in the Storstrømmen ice stream development, it is
712 quite possible that these glacial lineations in Store Bælt represent a period when a branch of the
713 ice stream began conforming to topographical controls (~~e.g.e.g.~~, Store Koldewey) and flowed
714 towards the south. At this point the ice may have flowed in to the southeast through Dove Bugt
715 Trough, ~~potentially also reaching the shelf break~~ (Fig. 9a).

716 ~~It is also possible that these MSGL formed during a glacial advance that followed the LGM (e.g.~~
717 ~~(Fig. 9b). Terrestrial moraines identified across the study area have been linked to different~~





719

720 *Figure 9. Maps showing ice sheet extent and advancement/retreat directions in SW Dove Bugt and Bessel Fjord*
 721 *during a range of periods. (a) during the LGM, The interpreted position of the ice sheet during the LGM. (b) The*
 722 *theoretical position of ice in Bessel Fjord and Dove Bugt during the Younger Dryas. during the Younger Dryas-(c-&d)*
 723 *~11.4-ka The ice position in Bessel Fjord at ~11.4 ka based on approximated deglaciation date presented in this*
 724 *study and the position and radiocarbon date for gravity core HH17-1309. (e) ~7.2 ka and (f) the Late Holocene. The*
 725 *black arrows in c-f represent the general direction of ice advancement/retreat. The size of ice caps in c-f are only*
 726 *indicative. Grey and purple-red colors in front of glaciers represent sediment input from over and under-flows. Purple*
 727 *dashed arrows represent the potential source of purple-red sediment found in Store Bælt. (d) The position of ice in*
 728 *Bessel Fjord at ~9.2 based on approximated deglaciation data from this study. (e) Ice retreating beyond our gravity*
 729 *core (HH17-1290) at ~7.1 ka during the HTM. (f) The Late Holocene ice expansion in Bessel Fjord with a radiocarbon*
 730 *date from gravity core HH17-1289. Background bathymetry displayed using IBCAO data (Jakobsson et al., 2020).*

731 An alternative interpretation, that cannot be excluded, is that these MSGs formed during a
732 glacial re-advance that followed the LGM. glacial events (Fig. 10a), including the Nanok II
733 Stadial, which is believed to have formed during the Younger Dryas (12.9–11.7 ka BP)
734 (Vasskog et al., 2015). Between Hochstetter Forland and Shannon Ø a submerged moraine
735 has been identified in Shannon Sound, which may indicate that at one point, possibly during the
736 Younger Dryas, the ice stream travelled south rather than through Dove Bugt Trough (Figs. 9b
737 & 10a; Hjort, 1981; Landvik, 1994; Larsen et al., 2016; Funder et al., 2021). (Hjort, 1981;
738 Landvik, 1994) Larsen et al. (2016) placed the ice margin at the Shannon Sound moraine, as
739 well as across Store Koldewey, Hochstetter Forland, and Shannon Ø giving it an age within late
740 Allerød/early Younger Dryas. Later, (Funder et al., 2021) excluded the moraines at Store
741 Koldewey as part of the ice margin and placed the margin within late Younger Dryas (Fig. 9b).
742 However, onshore deglaciation ages in Store Koldewey, Germania Land and Trums Ø, do not
743 support an ice advance during the Younger Dryas (Fig. 10b; see below). This was possibly an
744 ice readvance of the GIS outlet(s) (Soranebræen, L. Bistrup Bræ and/or Storstrømmen)
745 through western, inner Dove Bugt (Fig. 9b), where the surroundings (onshore and offshore)
746 were not or less affected. If this is correct, the readvance may have occurred during the
747 Younger Dryas (prior to 11.4 ka cal BP, see below). These ice margin interpretations are further
748 supported by the proposed deglaciation date of Store Bælt at ~11.2 ka, which follows the
749 Younger Dryas (see below).

750

751 **5.2. Ice Sheet retreat through Store Bælt**

752 The change from glacial marine and glacier front proximal mud (unit 1.1) in core HH17-1309 to
753 glacial marine glacier front distal (unit 1.2) represent a “transition zone” marking the deglaciation in
754 the region (Figs. 7 & 8e). The deglaciation has been dated to ~11.2 ka (Table 4).

755 This deglaciation age of 11.42 ka cal BP (Table 5) from Store Bælt immediately east of the
756 Bessel fjord entrance is attributed to the retreat of a N-S bound branch of the NEGIS (Fig. 9c)
757 rather than a W-E flowing ice body from Bessel Fjord (e.g. Fig 9d) due to the presence of N-S
758 oriented glacial lineations near the gravity core and a lack of morainal features that would
759 provide evidence for an W-E bound GIS or ice caps encroaching on Dove Bugt. This date,
760 represents a minimum age for the deglaciation as it however, is not from the base of the
761 deglacial deposits. and therefore represents a minimum age for the deglaciation of the inner
762 fjord. Previously published dates constraining the timing of deglaciation in Dove Bugt have been
763 restricted to terrestrial regions (Fig. 10b). Using cosmogenic nuclide dating, Skov et al., (2020)
764 produced deglaciation ages of ca. 12.7 ka cal BP at Store Koldewey and ca. 9.8 ka cal BP at
765 Pusterdal and later Larsen et al. (2022) produced a number of deglaciation ages across Dove
766 Bugt and Bessel Fjord (8.6-12.8 ka cal BP) (Fig. 10b). with the application of cosmogenic
767 nuclide dating on low to mid-elevation (100-460 m) bedrock. Further north, in eastern North
768 Greenland, Larsen et al. (2020) found that ice in deep fjords retreated rapidly from the outer
769 coast to the present ice margin between ~11 and 10 ka.

770 Our minimum age of ~11.4 ka cal BP from HH17-1309 largely matches findings in Dove Bugt
771 and Hochstetter Forland (Fig. 10b). It is slightly later than cosmogenic nuclide ages obtained
772 from Larsen et al. (2022) on Trums Ø (12.6 ka cal BP) and a Nanok moraine on southern Store
773 Koldewey (12.7 ka cal BP), but earlier than a second Store Koldewey Nanok moraine (11.0 ka
774 cal BP) as well as positions closer to the modern ice margin of Storstrømmen, such as Licht Ø

775 (10.8 ka cal BP) and Bræ Øerne (8.9 ka cal BP). Thus, Store Koldewey, and Trums Ø may have
776 been partially deglaciaded slightly prior to the final retreat of the NEGIS through Store Bælt.

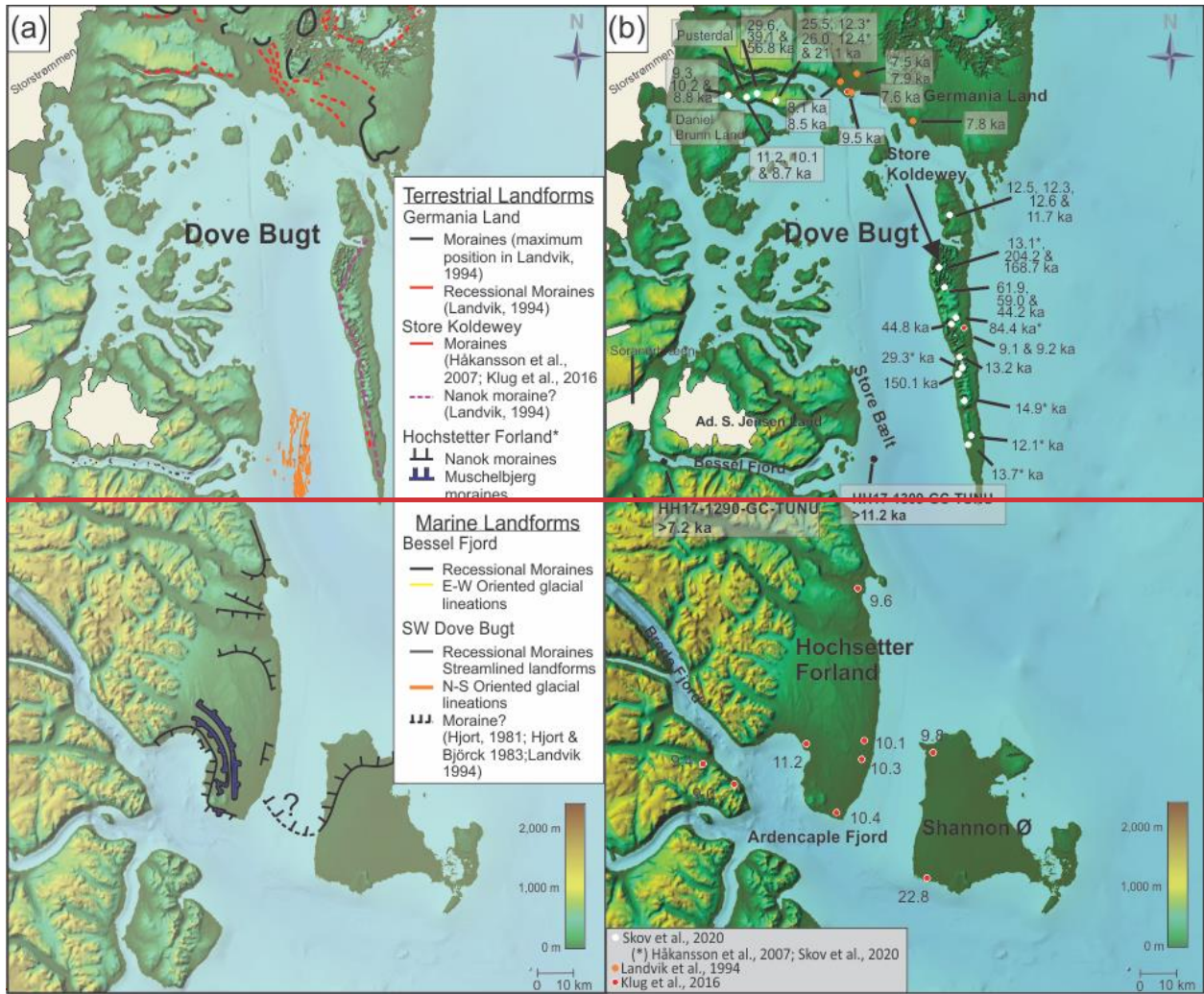
777

778 Radiocarbon dates obtained from lake sediments on Store Koldewey suggest that the earliest
779 onset of warmth may have begun around ~10 ka cal BP (Klug et al., 2009), therefore, the
780 deglaciaded of the area beginning just prior to this may further support these results.
781 Additionally, (Landvik, (1994) produced a range of deglaciaded ages between 9.6 to 8.5 ka cal
782 BP along the northern coast of Dove Bugt (Hvalrosodden and Snenæs on Germania Land) and
783 (Hjort, (1981, 1979) provided a range of delegation ages between 10.6 to 9.8 ka cal BP on
784 Hochstetter Forland. Later (Björck et al., (1994), on Hochstetter Forland, dated *Hiatella arctica*
785 shells near the shore of Peters Bugt Sø and *Portlandia arctica* shells in a delta distal to a Nanok
786 I ridge to 10.4 and 11.3 ka cal BP, respectively (Table 3; Fig. 10b).

787 ~~Bennike & Weidick (2001) compiled previously published radiocarbon dates that represent the~~
788 ~~minimum date for deglaciaded across Northeast Greenland. On the southern coast of Germania~~
789 ~~Land a minimum age of 9.5 ka BP has been presented (Bennike & Weidick, 2001), although~~
790 ~~earlier studies on Germania Land suggest that the ice front may have been east of the present~~
791 ~~day coastline until 19 ka BP and retracted to its current position by 7.5 ka BP (Landvik, 1994;~~
792 ~~Weidick et al., 1996). On Hochstetter Forland, (Bennike and Weidick, 2001) presented a~~
793 ~~minimum age of 11.2 ka, although a later study by (Klug et al., 2016) presented a larger range~~
794 ~~of deglaciaded ages for Hochstetter Foland and other nearby regions (Fig. 10b).~~

795 ~~The radiocarbon date of ~11.2 ka from HH17-1309 largely matches findings on Store Koldewey~~
796 ~~and Hochstetter Forland (Skov et al., 2020; Bennike and Weidick, 2001). It is slightly earlier to~~
797 ~~those obtained by Larsen et al. (2020) on the outer coast and deep fjords in eastern North~~
798 ~~Greenland, which placed the deglaciaded between 11 and 10 ka. Store Koldewey may have~~
799 ~~been partially deglaciaded prior to the retreat of the NGIS through Store Bælt, where Hochstetter~~
800 ~~Forland may have been fully or partially glaciaded.~~

801





803

804 *Figure 10. (a) Marine moraine ridges and glacial lineations from the current study together with previously mapped*
 805 *marine and terrestrial features. (b) Location of the current marine radiocarbon deglaciation dates from this study*
 806 *(Table 5) and previous publications. See Table 3 for recalibrated radiocarbon dates. are indicated by filled black*
 807 *circles. H: Hjort Lake, D: Duck Lake. Background displayed using IBCAO data (Jakobsson et al., 2020).*

808 Although based on a limited data set, the lack of prominent morainal landforms in Store Bælt
 809 may also suggest a rapid retreat through the region. A small number of retreat moraines have
 810 been observed in an isolated region of the study area, but the most prominent geomorphic
 811 landforms are glacial lineations. Placing Store Bælt within the context of Dowdeswell et al.
 812 (2008)'s proposed model for ice streams in high latitudes, ice likely retreated through the area
 813 rapidly, although the presence of small moraines may suggest brief periods of stagnation. This
 814 is in accordance with findings by (Larsen et al., 2020, 2022) Larsen et al. (2020) that deep
 815 fjords and outer regions in eastern North Greenland were rapidly deglaciated between ~12.64
 816 and 10 ka cal BP. However, additional data is required to confirm this.

817 Oceanic warming is believed to have contributed to the deglaciation of the inner shelf further
 818 north and south of Dove Bugt (e.g., Jackson et al., 2022; Davies et al., 2022). Within the study
 819 area, Store Koldewey does largely block oceanic water from the shelf from entering Store Bælt,
 820 however, it is possible that warmer water traveled through the Dove Bugt Trough to the south
 821 and impacted a north-south branch of the ice stream. This mechanism for warm water transport

822 has also been suggested for other east Greenland troughs (Arndt et al., 2015) and used to
823 explain how warm water has reached other outlets of the NEGIS (e.g., Zachariae Isstrøm via
824 the Norske Trough (Schaffer et al., 2017)).

825 5.3. Ice Sheet retreat through Bessel Fjord

826 ~~The appearance of recessional moraines in Bessel Fjord suggests that the fjord underwent a~~
827 ~~stepwise deglaciation. The large moraine identified between Basin 3 and Basin 4 (M3; Fig. 7e)~~
828 ~~is believed to have formed during a major ice halt or readvance. Smaller moraines occasionally~~
829 ~~follow topographic boundaries, which may suggest that the retreat of ice in Bessel Fjord was~~
830 ~~also partly topographically controlled. Recessional moraines identified by Olsen et al (2020) east~~
831 ~~of Dove Bugt in Store Koldewey contain a similar height to those identified here (excluding M3),~~
832 ~~however moraines identified on the shelf appear more numerous and are wider, likely due to the~~
833 ~~lack of topographic confinement.~~

834 ~~If the deglaciation of the fjord started immediately after the deglaciation of Store Belt, the~~
835 ~~radiocarbon date of ~11.2 ka from HH17-1309 represent a maximum age for the onset of the~~
836 ~~deglaciation of Bessel fjord. Cosmogenic nuclide dates from Trums Ø suggest that the~~
837 ~~deglaciation of the outer fjord began around 12.6 ka cal BP.~~ Gravity core HH17-1290, collected
838 from the inner fjord region, consists of sediments that reflect an increasingly ice distal
839 environment up core. One radiocarbon date from the core provides a minimum age of ~7.12 ka
840 cal BP for the deglaciation of Soranerbræen and/or local ice caps from the inner fjord region
841 (Table 5-4 & Fig. 9e). This date, however, is not from the base of the deglacial deposits and
842 therefore represents a minimum age for the deglaciation of the inner fjord. New cosmogenic
843 nuclide dates from Vandrepasset (onshore innermost Bessel fjord area, connecting the fjord and
844 the next valley to the south) provide an age of 8.6 ka cal BP for the deglaciation of the
845 innermost fjord area (Larsen et al., 2022), confirming this interpretation. This Our minimum age
846 of 7.12 ka cal BP and the results of Larsen (2022) falls within a modelled ice sheet extent by
847 Lecavalier et al. (2014) which placed the position of the ice sheet in the middle of Bessel Fjord
848 at 9 ka cal BP and that the present-day ice margin is reached by 6 ka cal BP. The minimum age
849 also agrees with the onset of HTM on Store Koldewey (~8.0 to 4.0 ka cal BP) (Wagner et al.,
850 2008; Klug et al., 2009; Schmidt et al., 2011) and Hochstetter Forland (8.8 and 5.6 ka cal BP)
851 (Björck & Persson, 1981; Björck et al., 1994), ~~while findings from Melles Lake suggest that the~~
852 ~~onset of warmth may have occurred earlier, at ~10 ka (Klug et al., 2009).~~ Thus, the GrIS
853 retreated from the marine realm in early Holocene, slightly before or at the time of the HTM in
854 this region (characterized by a mean July temperature 2-3°C higher than at present; Bennike et
855 al., 2008).

856 The appearance of recessional moraines in Bessel Fjord suggests that the fjord underwent a
857 stepwise deglaciation. The large moraine identified between Basin 3 and Basin 4 (M3; Fig. 7e)
858 is believed to have formed during a major ice halt or readvance, possibly climatically induced.
859 Smaller moraines occasionally follow topographic boundaries, which may suggest that the
860 retreat of ice in Bessel Fjord was also partly topographically controlled. Recessional moraines
861 identified by Olsen et al (2020) east of Dove Bugt in Store Koldewey Trough contain a similar
862 heights to those identified here (excluding M3). However, there are more moraines identified
863 in Store Koldey Trough than in Bessel Fjord on the shelf appear more numerous, and they are
864 wider, which is likely due to the lack of topographic confinement.

865 A decrease in atmospheric temperatures in early Holocene is recorded in the Greenland
866 Summit temperature records and includes the Preboreal Oscillation, the 9.2 ka event, the Pre-

867 8.2 ka cooling, and the 8.2 ka event, with the 8.2 ka event being the largest hemispheric-wide
868 negative temperature excursion during the Holocene (Kobashi et al., 2017). We tentatively
869 suggest that some of the moraines identified in the Bessel fjord may have developed during
870 some of these events. From this we suggest that increased Northern Hemisphere summer
871 insolation that peaked in the early Holocene was the main control for this part of the deglaciation
872 during which the ice front receded from the coastline to the west of (onshore) Bessel Fjord, a
873 distance of ~60 km. Assuming that this occurred over a maximum period of ~4.3 ka cal BP
874 (11.42 – 7.12 ka cal BP, ~~however, likely over a shorter period,~~ see discussion above on the
875 timing and length of this period), this corresponds to an average ice recession rate of ~145 m/yr.
876 This rate, a minimum rate, is considered realistic as it is half (or less) than the rate estimated
877 from the Nioghalvfjerdingsfjorden further north (also part of the Storstrømmen ice stream) where a
878 rate of ~30 – 40 m/yr was reported (Bennike & Björck, 2002).

879 Applying this minimum rate to the distance between Trums Ø (Larsen, et al., (2022); 12.6 ka cal
880 BP) and the major mounds and moraines identified in this study (M1, M2, M3 & M6), yields the
881 approximate minimum ages of 11.4, 10.5, 9.7 and 9.2 ka, respectively. This places
882 Soranerbræen between large moraine M3 and the bedrock mound M6 around the 9.2 ka event
883 (Fig. 9d). This is noteworthy as M3, and other many of the smaller moraines identified between
884 these two features, may have formed during this climatically cooler period. Additionally, many
885 smaller moraines in the fjord follow topographic boundaries, which may suggest that the retreat
886 of ice in Bessel Fjord was partly topographically controlled.

887 While oceanic warming may be partially responsible for the retreat of the NEGIS through Store
888 Bælt, we believe that Bessel Fjord is too sheltered by the sill at its entrance to have allowed
889 warm, intermediate water to enter and make a significant impact of the deglaciation of the
890 southern outlet of Soranerbræen. Our bathymetric dataset reveals that the depth of the sill is
891 between ~50 to 200 m, however large parts of it are above water and form islands. This is far
892 shallower than other fjord sills in the region that are theorized to have blocked warm Atlantic
893 Water (e.g., the sill in Dijnphna Sund to the north, which has a maximum depth of 170 m
894 (Wilson and Straneo, 2015)). Also, the effect of the glacio-eustatic readjustment is considered to
895 be small for this region, ~9.5 m higher in the Young Sound region (slightly south of our study
896 area) 7500 years ago (Pedersen et al., 2011). Rignot et al. (2022) also theorized that seafloor
897 topography may impact whether warm water is reaching the northern outlet of Soranerbræen.
898 They suggested further that the grounding line retreat of Storstrømmen, L. Bistrup Bræ, and
899 possibly Soranerbræen, may primarily be caused by ice thinning from atmospheric warming
900 (Rignot et al., 2022). We suggest that a similar mechanism may be responsible for
901 Soranerbræen's retreat through Bessel fjord during the deglaciation.

902 5.4. *Holocene glacier variability and sedimentary processes in Dove Bugt*

903 Sedimentological evidence (~~e.g.e.g., rhythmically~~-laminated muds) from HH17-1309 suggests,
904 that suspension settling from a glacial source(s) likely dominated southwestern Dove Bugt
905 during the Holocene. The contribution of sediment from the NEGIS seems unlikely, as Pusterdal
906 became deglaciated by 9.5 ka cal BP (Skov et al., 2020) and Storstrømmen retreated beyond
907 Bræ Øerne by 8.9 ka cal BP to its modern-day position by 7.5 ka BP (Larsen et al.,
908 2022) (~~Weidick et al., 1994~~), therefore it very well may be from Soranerbræen, or ~~perhaps more~~
909 ~~likely,~~ local ice caps. ~~It is possible that local ice caps and/or Soranerbræen advanced during~~
910 ~~short lived, cold reversals (i.e. ~11.4, 9.3, and 8.2 ka BP) (Rasmussen et al., 2007; Vasskog et~~
911 ~~al., 2015) or had a delayed response to warming, which may have contributed to the deposition~~

912 ~~of additional sediment in Store Bælt (see below for add conjecture concerning ice cap~~
913 ~~fluctuations).~~

914 During the latter part of the HTM in the middle Holocene, a time period in which some glaciers
915 are believed to have reached their minimum extent across Greenland, the NEGIS is believed to
916 have retreated beyond its current position between ~~5.46~~ to 1.2 ka cal BP (Table 3), creating the
917 Storstrømmen Sound (Weidick et al., 1994). Relating the core sedimentology to a linear age
918 model developed from sedimentation rates (~~i.e.i.e.~~, Table 5-4), laminations appear less
919 frequently in core HH17-1309 during this period, yet they are not absent. Laminations are
920 entirely absent in the Bessel Fjord core HH17-1290 during this period and remain absent
921 through the colder Late Holocene. ~~Later, During the Little Ice Age, Storstrømmen is believed~~
922 ~~demonstrated~~ to have expanded to its modern day position (Weidick et al., 1994).

923 Gravity core HH17-1289, collected to the north of an onshore glaciofluvial channel connected to
924 a modern-day ice cap, transitions to complex assortment of sand layers just prior to ~~3,596 3,544~~
925 cal yr BP (Fig. 7). Sedimentological evidence suggests that these sand layers are largely the
926 result of rapid, short lived depositional events (~~i.e.i.e.~~, turbidity currents) interpreted to be related
927 to the growth of a delta slightly south of the core site, from glaciofluvial sediment input from a
928 nearby outlet glacier.

929 ~~Pollen assemblage data from Hochstetter Forland mark the end of the HTM at 5.6 yr BP (Björck~~
930 ~~and Persson, 1981; Björck et al., 1994) and information derived from aquatic organisms mark~~
931 ~~the end of the HTM on Store Koldewey at 4 yr BP (Wagner et al., 2008; Klug et al., 2009b;~~
932 ~~Schmidt et al., 2011). Exposure dates in the region show that the HTM ended between 5.6-4 yr~~
933 ~~BP in this area (Briner et al., 2016). This coinciding~~ with the onset of turbidites in core HH17-
934 1289. Therefore, it is possible that this shift to sand dominated sedimentation within this core
935 was controlled by climatically driven processes. This onset is here suggested to result from
936 higher sediment input through the channel as local ice caps expanded outwards following the
937 HTM, possibly in response to this climate cooling (Fig. 9f). This period of cooling also
938 corresponds to extended concentrations of sea ice on the shelf (Kolling et al., 2017). ~~There is~~
939 ~~however an absence of sedimentological data in the Inner Fjord region to suggest that~~
940 ~~Soranerbræen readvanced beyond its modern-day position during the Late Holocene (Fig. 7).~~

941 ~~5.5. — Sea ice cover during the Holocene~~

942 ~~Lake studies suggest that the HTM occurred between ~8 and 4 ka on Store Koldewey (or as~~
943 ~~early as ~10 ka) (Wagner et al., 2008; Klug et al., 2009; Schmidt et al., 2011; Briner et al., 2016)~~
944 ~~and between 8.8 and 5.6 ka on Hochstetter Forland (Björck & Persson, 1981; Björck et al.,~~
945 ~~1994). Corresponding to the HTM in Bessel fjord, one would expect to see less sea ice and~~
946 ~~higher marine productivity. However, this is not reflected in the Ca/Fe ratios. Instead, Ca/Fe~~
947 ~~ratios are decreasing between 8.5 ka to 1 ka and only increase slightly thereafter, without any~~
948 ~~peak corresponding to an increased marine productivity during the HTM.~~

949 ~~The decrease in values up core in Bessel Fjord may represent a decrease in palaeo-productivity~~
950 ~~and an increase in sea ice cover over time. If this is the case, the HTM is not reflected in the~~
951 ~~Ca/Fe ratios, which either implies that Bessel Fjord was gradually covered in sea ice for a larger~~
952 ~~part of the year throughout the Holocene (~10 months a year at present) or that Ca/Fe ratios do~~
953 ~~not reflect sea ice conditions within the fjord, or the lack thereof. Further studies are needed to~~
954 ~~clarify this. Minor fluctuations in Ca/Fe ratios near the base of HH17-1290, and peak (or the~~

955 absence of peaks) identified throughout HH17-1289 reflect turbidite deposition, as Ca/Fe ratios
956 can be effective in distinguishing between turbidites and pelagites (Rothwell et al., 2006).

957 6. Conclusion

958 In summary:

- 959 • Glacial lineations (MSGLs) identified in SW Dove Bugt suggest fast-flowing ice,
960 interpreted to be from the NEGIS, developed during the LGM or an ice readvance during
961 the deglaciation or at a later (deglacial) ice readvance.
- 962 • Our minimum deglaciation date for Store Bælt (>11.4 ka cal BP) is slightly later than
963 new cosmogenic nuclide dates found onshore on Trums Ø and one of two Nanok
964 stadials on Store Koldewey (Larsen et al., 2022) as well as various other dates across
965 Store Koldewey (e.g., Skov et al., 2020). Thus, Store Koldewey and Trums Ø may have
966 been partially deglaciated prior to the final retreat of the NEGIS through Store Bælt.
- 967 • ~~The timing of this deglaciation (>11.2 ka) from this study is later than recent deglaciation~~
968 ~~dates from the island of Store Koldewey (Skov et al., 2020) but are in conformity or~~
969 ~~earlier than deglaciation dates on Hochstetter Forland slightly south of the study area~~
970 ~~(Klug et al., 2016).~~
- 971 • ~~Deglaciation of the Bessel Fjord is interpreted to have started immediately after the~~
972 ~~deglaciation of Dove Bugt, i.e., < 11.2 ka (in the Preboreal).~~
- 973 • Moraines in Bessel Fjord (to the west of Dove Bugt) suggests that the fjord underwent
974 multiple halts/or readvances upon deglaciation. Thus, the bathymetry of Bessel Fjord ~~(to~~
975 ~~the west of Dove Bugt)~~ indicates that the glacial dynamics of the fjord were more
976 dynamic than onshore evidence suggests.
- 977 • The radiocarbon date of 7.12 ka cal BP obtained in an inner fjord core is interpreted as a
978 minimum age at which Soranerbræen retreated to or beyond its present-day onshore
979 position west of the fjord and is in conformity with cosmogenic nuclide dates presented
980 by Larsen et al. (2022) in the onshore inner fjord (8.6 ka cal BP).
- 981 • Ice recession in Bessel Fjord occurred at a minimum average rate of ~145 m/yr.
- 982 • The GrlS retreated from the marine realm in the early Holocene, around the time of the
983 onset of the Holocene Thermal Maximum HTM in this region. ~~From this we suggest that~~
984 ~~increased Northern Hemisphere summer insolation that peaked in the early Holocene~~
985 ~~was the main control for this part of the deglaciation (the mean July temperature then~~
986 ~~was according to Bennike et al. (2008) at least 2-3 °C higher than at present).~~
- 987 • A low sedimentation rate of 13.6355 cm/ka after 7.12 ka cal BP in HH17-1290, and the
988 presence of only massive mud, suggests that Soranerbræen did not expand back into
989 Bessel Fjord for the remainder of the Holocene.
- 990 • The transition of mud to muddy sand at 4 ka cal BP in a mid-fjord core HH17-1289 may
991 provide evidence for local ice cap growth. Thus, ice caps in Bessel Fjord ~~were~~ may have
992 fluctuated with greater sensitivity to climatic conditions than the NE sector of the GrlS
993 during the cooling phase that followed the HTM.

994
995 *Data availability:* The bathymetry and core data from UiT The Arctic University of Norway will be
996 available upon reasonable request at UiT's open research data repository:
997 <https://dataverse.no/dataverse/uit>.

998 *Author contributions:* Jan Sverre Laberg and Tom Arne Rydningen designed this study and
999 collected the new data during the 2017 TUNU VII cruise. The bathymetrical and lithological data
1000 were interpreted by Kevin Zoller in collaboration with Jan Sverre Laberg and Tom Arne
1001 Rydningen. Kevin Zoller prepared the manuscript with contributions from all co-authors.

1002 *Competing interests:* The authors declare that they have no conflict of interest.

1003 *Acknowledgement:* We would like to thank the participants of the 2017 TUNU cruise to
1004 Greenland for making this project possible. A special thanks to the captain and crew of the RV
1005 *Helmer Hanssen* for their involvement in the cruise and assistance in collecting the data. A
1006 thanks also goes out to the lab staff at UiT, Trine Dahl, Karina Monsen and Ingvild Hald, who
1007 assisted with processing sediment core samples for this project. We would also like to thank
1008 Gesine Mollenhauer and the lab staff at the Alfred Wegener Institut for providing us with
1009 radiocarbon dated material using their MICADAS. Funding for this work was provided by UiT
1010 The Arctic University of Norway.

1011

1012 **References**

1013 Arndt, J. E.: Marine geomorphological record of Ice Sheet development in East Greenland since
1014 the Last Glacial Maximum, *J. Quat. Sci.*, 33, 853–864, <https://doi.org/10.1002/jqs.3065>, 2018.

1015 Arndt, J. E., Jokat, W., Dorschel, B., Mykleburst, R., Dowdeswell, J. A., and Evans, J.: A new
1016 bathymetry of the Northeast Greenland continental shelf: Constraints on glacial and other
1017 processes, *AGU Publ. Geochemistry Geophys. Geosystems*, 16, 267–300,
1018 <https://doi.org/10.1002/2014GC005684>.Key, 2015.

1019 Arndt, J. E., Jokat, W., and Dorschel, B.: The last glaciation and deglaciation of the Northeast
1020 Greenland continental shelf revealed by hydro-acoustic data, *Quat. Sci. Rev.*, 160, 45–56, 2017.

1021 Batchelor, C. L., Dowdeswell, J. A., and Rignot, E.: Submarine landforms reveal varying rates
1022 and styles of deglaciation in North-West Greenland fjords, *Mar. Geol.*, 402, 60–80,
1023 <https://doi.org/10.1016/j.margeo.2017.08.003>, 2018.

1024 Bennike, O. and Björck, S.: Chronology of the last recession of the Greenland Ice Sheet, *J.*
1025 *Quat. Sci.*, 17, 211–219, <https://doi.org/10.1002/jqs.670>, 2002.

1026 Bennike, O. and Weidick, A.: Late Quaternary history around Nioghalvfjerdingsfjorden and
1027 Jøkelbugten, North-East Greenland, *Boreas*, 30, 205–227, <https://doi.org/10.1111/j.1502-3885.2001.tb01223.x>, 2001.

1029 Bennike, O., Sørensen, M., Fredskild, B., Jacobsen, B. H., Böcher, J., Amsinck, S. L.,
1030 Jeppesen, E., Andreasen, C., Christiansen, H. H., and Humlum, O.: Late Quaternary
1031 Environmental and Cultural Changes in the Wollaston Forland Region, Northeast Greenland,
1032 *Adv. Ecol. Res.*, 40, 45–79, [https://doi.org/10.1016/S0065-2504\(07\)00003-7](https://doi.org/10.1016/S0065-2504(07)00003-7), 2008.

1033 Bentley, C. R.: Antarctic ice streams: a review, *Geophys. Res.*, 92(6), 8843–8858, 1987.

1034 Biette, M., Jomelli, V., Chenet, M., Braucher, R., Rinterknecht, V., and Lane, T.: Mountain
1035 glacier fluctuations during the Lateglacial and Holocene on Clavering Island (northeastern
1036 Greenland) from ¹⁰Be moraine dating, *Boreas*, 49, 873–885, <https://doi.org/10.1111/bor.12460>,
1037 2020.

- 1038 Björck, S. and Persson, T.: Late Weichselian and Flandrian biostratigraphy and chronology from
1039 hochstetter forland, northeast Greenland, *Medd. Om. Grøn. Geosci.*, 5, 1–19, 1981.
- 1040 Björck, S., Wohlfarth, B., Bennike, O., Hjort, C., and Persson, T.: Revision of the early Holocene
1041 lake sediment based chronology and event stratigraphy on Hochstetter Forland, NE Greenland,
1042 *Boreas*, 23, 513–523, <https://doi.org/10.1111/j.1502-3885.1994.tb00619.x>, 1994.
- 1043 Boulton, G. S. and Deynoux, M.: Sedimentation in glacial environments and the identification of
1044 tills and tillites in ancient sedimentary sequences, *Precambrian Res.*, 15, 397–422,
1045 [https://doi.org/10.1016/0301-9268\(81\)90059-0](https://doi.org/10.1016/0301-9268(81)90059-0), 1981.
- 1046 Boulton, G. S., Hagdorn, M., and Hulton, N. R. J.: Streaming flow in an ice sheet through a
1047 glacial cycle, *Ann. Glaciol.*, 36, 117–128, <https://doi.org/10.3189/172756403781816293>, 2003.
- 1048 Briner, J. P., McKay, N. P., Axford, Y., Bennike, O., Bradley, R. S., de Vernal, A., Fisher, D.,
1049 Francus, P., Fréchette, B., Gajewski, K., Jennings, A., Kaufman, D. S., Miller, G., Rouston, C.,
1050 and Wagner, B.: Holocene climate change in Arctic Canada and Greenland, *Quat. Sci. Rev.*,
1051 147, 340–364, <https://doi.org/10.1016/j.quascirev.2016.02.010>, 2016.
- 1052 Cartigny, M. J. B., Postma, G., Berg, J. H., and Mastbergen, D. R.: A comparative study of
1053 sediment waves and cyclic steps based on geometries, internal structures and numerical
1054 modeling, *Mar. Geol.*, 280, 40–56, 2011.
- 1055 Christiansen, J. S.: The TUNU-Programme : Euro-Arctic Marine Fishes — Diversity and
1056 Adaptation, in: *Adaptation and Evolution in Marine Environments*, vol. 1, 35–50,
1057 <https://doi.org/10.1007/978-3-642-27352-0>, 2012.
- 1058 Clark, C. D.: Mega-scale lineations and cross-cutting ice-flow landforms, *Earth Surf. Process.*
1059 *Landforms*, 18, 1–29, 1993.
- 1060 Clark, C. D. and Stokes, C. R.: Palaeo-ice stream landsystem, in: *Glacial Landscapes*, edited
1061 by: Evans, D. J. A., Edward Arnold, London, 204–227, 2003.
- 1062 Clark, C. D., Tulaczyk, S. M., Stokes, C. R., and Canals, M.: A groove-ploughing theory for the
1063 production of mega-scale glacial lineations, and implications for ice-stream mechanics, *J.*
1064 *Glaciol.*, 49, 240–256, <https://doi.org/10.3189/172756503781830719>, 2003.
- 1065 Cohen, J., Screen, J. A., Furtado, J. C., Barlow, M., Whittleston, D., Coumou, D., Francis, J.,
1066 Dethloff, K., Entekhabi, D., Overland, J., and Jones, J.: Recent Arctic amplification and extreme
1067 mid-latitude weather, *Nat. Publ. Gr.*, 7, 627–637, <https://doi.org/10.1038/ngeo2234>, 2014.
- 1068 Cowan, E. A., Seramur, K. C., Cai, J., and Powell, R. D.: Cyclic sedimentation produced by
1069 fluctuations in meltwater discharge, tides and marine productivity in an Alaskan fjord,
1070 *Sedimentology*, 46, 1109–1126, <https://doi.org/10.1046/j.1365-3091.1999.00267.x>, 1999.
- 1071 Cremer, H., Bennike, O., and Wagner, B.: Lake sediment evidence for the last deglaciation of
1072 eastern Greenland, *Quat. Sci. Rev.*, 27, 312–319,
1073 <https://doi.org/10.1016/j.quascirev.2007.09.004>, 2008.
- 1074 Davies, J., Mathiasen, A. M., Kristiansen, K., Hansen, K. E., Wacker, L., Alstrup, A. K. O., Munk,
1075 O. L., Pearce, C., and Seidenkrantz, M. S.: Linkages between ocean circulation and the
1076 Northeast Greenland Ice Stream in the Early Holocene, *Quat. Sci. Rev.*, 286, 107530,
1077 <https://doi.org/10.1016/j.quascirev.2022.107530>, 2022.
- 1078 Dowdeswell, J. A., Ottesen, D., Evans, J., Cofaigh, C. Ó., and Anderson, J. B.: Submarine
1079 glacial landforms and rates of ice-stream collapse, *Geology*, 36, 819–822,

- 1080 <https://doi.org/10.1130/G24808A.1>, 2008.
- 1081 Dowdeswell, J. A., Hogan, K. A., Ó Cofaigh, C., Fugelli, E. M. G., Evans, J., and Noormets, R.:
1082 Late Quaternary ice flow in a West Greenland fjord and cross-shelf trough system: submarine
1083 landforms from Rink Isbrae to Uummannaq shelf and slope, *Quat. Sci. Rev.*, 92, 292–309,
1084 2014.
- 1085 Dowdeswell, J. A., Canals, M., Jakobsson, M., Todd, B. J., Dowdeswell, E. K., and Hogan, K.
1086 A.: The variety and distribution of submarine glacial landforms and implications for ice-sheet
1087 reconstruction, *Geol. Soc. Mem.*, 46, 519–552, <https://doi.org/10.1144/M46.183>, 2016.
- 1088 Evans, J., Dowdeswell, J. A., Grobe, H., Niessen, F., Stein, R., Hubberten, H. W., and
1089 Whittington, R. J.: Late Quaternary sedimentation in Kejser Franz Joseph Fjord and the
1090 continental margin of East Greenland, *Geol. Soc. Spec. Publ.*, 203, 149–179,
1091 <https://doi.org/10.1144/GSL.SP.2002.203.01.09>, 2002.
- 1092 Evans, J., Ó Cofaigh, C., Dowdeswell, J. A., and Wadhams, P.: Marine geophysical evidence
1093 for former expansion and flow of the Greenland Ice Sheet across the north-east Greenland
1094 continental shelf, *J. Quat. Sci.*, 24, 279–293, 2009.
- 1095 Eyles, N., Eyles, C. H., and Niall, An. D.: Lithofacies types and vertical profile models; an
1096 alternative approach to the description and environmental interpretation of glacial diamict and
1097 diamictite sequences, *Sedimentology*, 30, 393–410, 1983.
- 1098 Folk, R. L.: The Distinction between Grain Size and Mineral Composition in Sedimentary-Rock
1099 Nomenclature, *J. Geol.*, 62, 344–359, 1954.
- 1100 Folk, R. L. and Ward, W.: Brazos river bar, a study in the significance of grain size parameters.,
1101 *J. Sediment. Petrol.*, 27, 34–59, 1957.
- 1102 Forwick, M. and Vorren, T. O.: Deglaciation history and post-glacial mass movements in
1103 Balsfjord, northern Norway, *Polar Res.*, 21(2), 259–266, 1998.
- 1104 Forwick, M. and Vorren, T. O.: Late Weichselian and Holocene sedimentary environments and
1105 ice rafting, *Palaeogeogr. Palaeoclimatol. Palaeoecol.*, 280, 258–274, 2009.
- 1106 Forwick, M., Vorren, T. O., Hald, M., Korsun, S., Roh, Y., Vogt, C., and Yoo, K. C.: Spatial and
1107 temporal influence of glaciers and rivers on the sedimentary environment in Sassenfjorden and
1108 Tempelfjorden, Spitsbergen, *Geol. Soc. London, Spec. Publ.*, 344, 163–193,
1109 <https://doi.org/10.1144/SP344.13>, 2010.
- 1110 Funder, S., Kjeldsen, K. K., Kjær, H. K., and Ó Cofaigh, C.: The Greenland Ice Sheet During the
1111 Past 300,000 Years: A Review, *Dev. Quat. Sci.*, 15, 699–713, <https://doi.org/10.1016/B978-0-444-53447-7.00050-7>, 2011.
- 1113 Funder, S., Sørensen, A. H. L., Larsen, N. K., Bjørk, A. A., Briner, J. P., Olsen, J., Schomacker,
1114 A., Levy, L. B., and Kjær, K. H.: Younger Dryas ice margin retreat in Greenland: new evidence
1115 from southwestern Greenland, *Clim. Past*, 17, 587–601, 2021.
- 1116 Geirsdóttir, Á., Hardardóttir, J., and Andrews, J. T.: Late-Holocene terrestrial glacial history of
1117 Miki and I.C. Jacobsen Fjords, East Greenland, *Holocene*, 10, 123–134,
1118 <https://doi.org/10.1191/095968300666213169>, 2000.
- 1119 Håkansson, L., Graf, A., Strasky, S., Ivy-ochs, S., Kubik, P. W., Hjort, C., Shlüchter, C.,
1120 Geografiska, S., Series, A., Geography, P., Hakansson, L., Graf, A., Strasky, S., Ivy-ochs, S.,
1121 Kubik, P. W., Hjort, C., and Schlichter, C.: Cosmogenic ¹⁰Be-Ages from the Store Koldewey

- 1122 Island, NE Greenland, *Geogr. Ann. Ser. A Phys. Geogr.*, 89, 195–202, 2007.
- 1123 Hansen, K. E., Lorenzen, J., Davies, J., Wacker, L., Pearce, C., and Seidenkrantz, M.-S.:
1124 Deglacial to Mid Holocene environmental conditions on the northeastern Greenland shelf,
1125 *Quaternary Sci. Rev.*, 293, 107704, 2022.
- 1126 Heaton, T. J., Köhler, P., Butzin, M., Bard, E., Reimer, R. W., Austin, W. E. N., Ramsey, C. B.,
1127 Grootes, P. M., Hughen, K. A., Kromer, B., Reimer, P. J., and Heaton, T. J.: Marine20 — The
1128 Marine Radiocarbon Age Calibration Curve (0-55,000 CAL BP), *Radio*, 62, 779–820,
1129 <https://doi.org/10.1017/RDC.2020.68>, 2020.
- 1130 Heaton, T. J., Bard, E., Ramsey, C. B., Butzin, M., Hatté, C., Hughen, K. A., Köhler, P., and
1131 Reimer, P. J.: A Response to Community Questions on the Marine20 Radiocarbon Age
1132 Calibration Curve: Marine Reservoir Ages and The Calibration of 14C Samples from the
1133 Oceans, *Radiocarbon*, 65, 247–273, <https://doi.org/10.1017/RDC.2022.66>, 2022.
- 1134 Higgins, A. K.: North Greenland Glaciers Velocities and Calf Ice Production, *Polarforschung*, 60,
1135 1–23, 1991.
- 1136 Hill, P. R.: Changes in submarine channel morphology and strata development from repeat
1137 multibeam surveys in the Fraser River delta, western Canada, in: *Sediments, Morphology and
1138 Sedimentary Processes on Continental Shelves*, edited by: Li, M. Z., Sherwood, C. R., and Hill,
1139 P. R., Blackwell Science, International Association of Sedimentologists, 47–70, 2012.
- 1140 Hjort, C.: Glaciation in northern East Greenland during the Late Weichselian and Early
1141 Flandrian, *Boreas*, 8, 281–296, <https://doi.org/10.1111/j.1502-3885.1979.tb00812.x>, 1979.
- 1142 Hjort, C.: A glacial chronology for northern East Greenland, *Boreas*, 10, 259–274, 1981.
- 1143 Hjort, C. and Björck, S.: A re-evaluated glacial chronology for Northern East Greenland, *Geol.
1144 Föreningen i Stock. Förhandlingar*, 105, 235–243, <https://doi.org/10.1080/11035898309452590>,
1145 1983.
- 1146 Hogan, K. A., Dowdeswell, J. A., Noormets, R., Evans, J., and Ó Cofaigh, C.: Evidence for full-
1147 glacial flow and retreat of the Late Weichselian Ice Sheet from the waters around Kong Karls
1148 Land, eastern Svalbard, *Quat. Sci. Rev.*, 29, 3563–3582,
1149 <https://doi.org/10.1016/j.quascirev.2010.05.026>, 2010.
- 1150 Hogan, K. A., Ó Cofaigh, C., Jennings, A. E., Dowdeswell, J. A., and Hiemstra, J. F.:
1151 Deglaciation of a major palaeo-ice stream in Disko Trough, West Greenland, *Quat. Sci. Rev.*,
1152 147, 5–26, 2016.
- 1153 Huddart, D. and Lister, H.: The Origin of Ice Marginal Terraces and Contact Ridges of East
1154 Kangerdluarssuk Glacier, SW Greenland, *Geogr. Ann.*, 63 A, 31–39, 1981.
- 1155 Jackson, R., Andreasen, N., Oksman, M., Andersen, T. J., Pearce, C., Seidenkrantz, M.-S., and
1156 Ribeiro, S.: Marine conditions and development of the Sirius Water polynya on the North-East
1157 Greenland shelf during the Younger Dryas-Holocene, *Quat. Sci. Rev.*, 291, 107647, 2022.
- 1158 Jakobsson, M., Hogan, K. A., Mayer, L. A., Mix, A., Jennings, A., Stoner, J., Eriksson, B.,
1159 Jerram, K., Mohammad, R., Pearce, C., Reilly, B., and Stranne, C.: The Holocene retreat
1160 dynamics and stability of Petermann Glacier in northwest Greenland, *Nat. Commun.*, 9,
1161 <https://doi.org/10.1038/s41467-018-04573-2>, 2018.
- 1162 Jakobsson, M., Mayer, L. A., Bringensparr, C., Castro, C. F., Mohammad, R., Johnson, P.,
1163 Ketter, T., Accettella, D., Amblas, D., An, L., Arndt, J. E., Canals, M., Casamor, J. L., Chauché,

- 1164 N., Coakley, B., Danielson, S., Demarte, M., Dickson, M. L., Dorschel, B., Dowdeswell, J. A.,
 1165 Dreutter, S., Fremand, A. C., Gallant, D., Hall, J. K., Hehemann, L., Hodnesdal, H., Hong, J.,
 1166 Ivaldi, R., Kane, E., Klaucke, I., Krawczyk, D. W., Kristoffersen, Y., Kuipers, B. R., Millan, R.,
 1167 Masetti, G., Morlighem, M., Noormets, R., Prescott, M. M., Rebesco, M., Rignot, E., Semiletov,
 1168 I., Tate, A. J., Travaglini, P., Velicogna, I., Weatherall, P., Weinrebe, W., Willis, J. K., Wood, M.,
 1169 Zarayskaya, Y., Zhang, T., Zimmermann, M., and Zinglensen, K. B.: The International
 1170 Bathymetric Chart of the Arctic Ocean Version 4.0, *Sci. Data*, 7, 1–14,
 1171 <https://doi.org/10.1038/s41597-020-0520-9>, 2020.
- 1172 Joughin, I., Fahnestock, M., MacAyeal, D., Bamber, J. L., and Gogineni, P.: Observation and
 1173 analysis of ice flow in the largest Greenland ice stream, *J. Geophys. Res. Atmos.*, 106, 34021–
 1174 34034, <https://doi.org/10.1029/2001JD900087>, 2001.
- 1175 Kelly, M. A., Lowell, T. V., Hall, B. L., Schaefer, J. M., Finkel, R. C., Goehring, B. M., Alley, R.
 1176 B., and Denton, G. H.: A ^{10}Be chronology of lateglacial and Holocene mountain glaciation in the
 1177 Scoresby Sund region, east Greenland: implications for seasonality during lateglacial time,
 1178 *Quat. Sci. Rev.*, 27, 2273–2282, 2008.
- 1179 Kempf, P., Forwick, M., Laberg, J. S., and Vorren, T. O.: Late Weichselian and Holocene
 1180 sedimentary palaeoenvironment and glacial activity in the high-arctic van Keulenfjorden,
 1181 Spitsbergen, *The Holocene*, 23 (11), 1607–1618, <https://doi.org/10.1177/0959683613499055>,
 1182 2013.
- 1183 Khan, S. A., Kjær, K. H., Bevis, M., Bamber, J. L., Wahr, J., Kjeldsen, K. K., Bjørk, A. A.,
 1184 Korsgaard, N. J., Stearns, L. A., Van Den Broeke, M. R., Liu, L., Larsen, N. K., and Muresan, I.
 1185 S.: Sustained mass loss of the northeast Greenland ice sheet triggered by regional warming,
 1186 *Nat. Clim. Chang.*, 4, 292–299, <https://doi.org/10.1038/nclimate2161>, 2014.
- 1187 King, E. C., Hindmarsh, R. C. A., and Stokes, C. R.: Formation of mega-scale glacial lineations
 1188 observed beneath a West Antarctic ice stream, *Nat. Geosci.*, 2, 585–588,
 1189 <https://doi.org/10.1038/ngeo581>, 2009.
- 1190 King, M. D., Howat, I. M., Candela, S. G., Noh, M. J., Jeong, S., Noël, B. P. Y., van den Broeke,
 1191 M. R., Wouters, B., and Negrete, A.: Dynamic ice loss from the Greenland Ice Sheet driven by
 1192 sustained glacier retreat, *Commun. Earth Environ.*, 1, 1–7, <https://doi.org/10.1038/s43247-020-0001-2>, 2020.
- 1194 Klages, J. P., Kuhn, G., Hillenbrand, C.-D., Graham, A. G. C., Smith, J. A., Larter, R. D., and
 1195 Gohl, K.: First geomorphological record and glacial history of an inter-ice stream ridge on the
 1196 West Antarctic continental shelf, *Quat. Sci. Rev.*, 61, 47–61, 2013.
- 1197 Klages, J. P., Kuhn, G., Graham, A. G. C., Hillenbrand, C.-D., Smith, J. A., Nitsche, F. O.,
 1198 Larter, R. D., and Gohl, K.: Palaeo-ice stream pathways and retreat style in the easternmost
 1199 Amundsen Sea Embayment, West Antarctica, revealed by combined multibeam bathymetric
 1200 and seismic data, *Geomorphology*, 245, 207–222, 2015.
- 1201 Klug, M., Schmidt, S., Melles, M., Wagner, B., Bennike, O., and Heiri, O.: Lake sediments from
 1202 Store Koldewey, Northeast Greenland, as archive of Late Pleistocene and Holocene climatic
 1203 and environmental changes, *Boreas*, 38, 59–71, <https://doi.org/10.1111/j.1502-3885.2008.00038.x>, 2009a.
- 1205 Klug, M., Bennike, O., and Wagner, B.: Repeated short-term bioproductivity changes in a
 1206 coastal lake on Store Koldewey, northeast Greenland: An indicator of varying sea-ice
 1207 coverage?, *Holocene*, 19, 653–663, <https://doi.org/10.1177/0959683609104040>, 2009b.

- 1208 Klug, M., Bennike, O., and Wagner, B.: Late Pleistocene to early Holocene environmental
1209 changes on Store Koldewey, coastal north-east Greenland, *Polar Res.*, 35,
1210 <https://doi.org/10.3402/polar.v35.21912>, 2016.
- 1211 Kobashi, T., Menviel, L., Jeltsch-Thömmes, A., Vinther, B. M., Box, J. E., Muscheler, R.,
1212 Nakaegawa, T., Pfister, P. L., Döring, M., Leuenberger, M., Wanner, H., and Ohmura, A.:
1213 Volcanic influence on centennial to millennial Holocene Greenland temperature change, *Sci.*
1214 *Rep.*, 7, 1–10, <https://doi.org/10.1038/s41598-017-01451-7>, 2017.
- 1215 Kolling, H. M., Stein, R., Fahl, K., Perner, K., and Moros, M.: Short-term variability in late
1216 Holocene sea ice cover on the East Greenland Shelf and its driving mechanisms, *Palaeogeogr.*
1217 *Palaeoclimatol. Palaeoecol.*, 485, 336–350, <https://doi.org/10.1016/j.palaeo.2017.06.024>, 2017.
- 1218 Krieger, L., Floricioiu, D., and Neckel, N.: Drainage basin delineation for outlet glaciers of
1219 Northeast Greenland based on Sentinel-1 ice velocities and TanDEM-X elevations, *Remote*
1220 *Sens. Environ.*, 237, 111483, <https://doi.org/10.1016/j.rse.2019.111483>, 2020.
- 1221 Laberg, J. S., Forwick, M., and Husum, K.: New geophysical evidence for a revised maximum
1222 position of part of the NE sector of the Greenland ice sheet during the last glacial maximum,
1223 *Arktos*, 3, <https://doi.org/10.1007/s41063-017-0029-4>, 2017.
- 1224 Lambeck, K., Rouby, H., Purcell, A., Sun, Y., and Sambridge, M.: Sea level and global ice
1225 volumes from the Last Glacial Maximum to the Holocene, *Proc. Natl. Acad. Sci.*, 111, 15296–
1226 15303, <https://doi.org/10.1073/pnas.1411762111>, 2014.
- 1227 Landvik, J. Y.: The last glaciation of Germania Land and adjacent areas, northeast Greenland,
1228 *J. Quat. Sci.*, 9, 81–92, <https://doi.org/10.1002/jqs.3390090108>, 1994.
- 1229 Lane, T. P., Roberts, D. H., Ó Cofaigh, C., Vieli, A., and Moreton, S. G.: The glacial history of
1230 the southern Svartehuk Halvø, West Greenland, *Arktos*, 1, 1–28,
1231 <https://doi.org/10.1007/s41063-015-0017-5>, 2015.
- 1232 Larsen, N. K., Funder, S., Linge, H., Möller, P., Schomacker, A., Fabel, D., Xu, S., and Kjær, K.
1233 H.: A Younger Dryas re-advance of local glaciers in north Greenland, *Quat. Sci. Rev.*, 147, 47–
1234 58, <https://doi.org/10.1016/j.quascirev.2015.10.036>, 2016.
- 1235 Larsen, N. K., Levy, L. B., Carlson, A. E., Buizert, C., Olsen, J., Strunk, A., Bjørk, A. A., and
1236 Skov, D. S.: Instability of the Northeast Greenland Ice Stream over the last 45,000 years, *Nat.*
1237 *Commun.*, 9, 3–10, <https://doi.org/10.1038/s41467-018-04312-7>, 2018.
- 1238 Larsen, N. K., Søndergaard, A. S., Levy, L. B., Olsen, J., Strunk, A., Bjørk, A. A., and Skov, D.:
1239 Contrasting modes of deglaciation between fjords and inter-fjord areas in eastern North
1240 Greenland, *Boreas*, 49, 905–919, <https://doi.org/10.1111/bor.12475>, 2020.
- 1241 Larsen, N. K., Søndergaard, A. S., Levy, L. B., Strunk, A., Skov, D. S., Bjørk, A., Khan, S. A.,
1242 and Olsen, J.: Late glacial and Holocene glaciation history of North and Northeast Greenland,
1243 *Arctic, Antarct. Alp. Res.*, 54, 294–313, <https://doi.org/10.1080/15230430.2022.2094607>, 2022.
- 1244 Levy, L. B., Kelly, M. A., Lowell, T. V., Hall, B. L., Howley, J. A., and Smith, C. A.: Coeval
1245 fluctuations of the Greenland ice sheet and a local glacier, central East Greenland, during late
1246 glacial and early Holocene time, *Geophys. Res. Lett.*, 43, 1623–1631, 2016.
- 1247 Lyså, A. and Vorren, T. O.: Seismic facies and architecture of ice-contact submarine fans in
1248 high-relief fjords, Troms, Northern Norway, *Boreas*, 26, 309–328, 1997.
- 1249 Mouginot, J., Rignot, E., Scheuchl, B., Fenty, I., Khazendar, A., Morlighem, M., Buzzi, A., and

- 1250 Paden, J.: Fast retreat of Zachariae Isstrom, Northeast Greenland, *Science* (80-.), 350, 1357–
1251 1361, 2015.
- 1252 Mouginit, J., Bjørk, A. A., Millan, R., Scheuchl, B., and Rignot, E.: Insights on the Surge
1253 Behavior of Storstrømmen and L. Bistrup Bræ, Northeast Greenland, Over the Last Century,
1254 *Geophys. Res. Lett.*, 45, 11,197-11,205, <https://doi.org/10.1029/2018GL079052>, 2018.
- 1255 Newton, A. M. W., Knutz, P. C., Huuse, M., Gannon, P., Brocklehurst, S. H., Clausen, O. R.,
1256 and Gong, Y.: Ice stream reorganization and glacial retreat on the northwest Greenland shelf,
1257 *Geophys. Res. Lett.*, 44, 7826–7835, <https://doi.org/10.1002/2017GL073690>, 2017.
- 1258 Ó Cofaigh, C.: Flow Dynamics and till genesis associated with a marin-based Antarctic palaeo-
1259 ice stream, *Quat. Sci. Rev.*, 24, 709–740, 2005.
- 1260 Ó Cofaigh, C., Dowdeswell, J. A., and Grobe, H.: Holocene glacimarine sedimentation, inner
1261 Scoresby Sund, East Greenland: The influence of fast-flowing ice-sheet outlet glaciers, *Mar.*
1262 *Geol.*, 175, 103–129, [https://doi.org/10.1016/S0025-3227\(01\)00117-7](https://doi.org/10.1016/S0025-3227(01)00117-7), 2001.
- 1263 Ó Cofaigh, C., Dowdeswell, J. A., Jennings, A. E., Hogan, K. A., Kilfeather, A., Hiemstra, J. F.,
1264 Noormets, R., Evans, J., McCarthy, D. J., Andrews, J. T., Lloyd, J. M., and Moros, M.: An
1265 extensive and dynamic ice sheet on the west greenland shelf during the last glacial cycle,
1266 *Geology*, 41, 219–222, <https://doi.org/10.1130/G33759.1>, 2013.
- 1267 Olsen, I. L., Forwick, M., Laberg, J. S., and Rydningen, T. A.: Last Glacial ice-sheet dynamics
1268 offshore NE Greenland – a case study from Store Koldewey Trough, *The Cryosphere*
1269 *Discussions*, 2020.
- 1270 Olsen, I. L., Laberg, J. S., Forwick, M., Rydningen, T. A., and Husum, K.: Late Weichselian and
1271 Holocene behavior of the Greenland Ice Sheet in the Kejser Franz Josef Fjord system, NE
1272 Greenland, *Quat. Sci. Rev.*, 2022.
- 1273 Ottesen, D., Dowdeswell, J. A., Benn, D. I., Kristensen, L., Christiansen, H. H., Christensen, O.,
1274 Hansen, L., Lebesbye, E., Forwick, M., and Vorren, T. O.: Submarine landforms characteristic of
1275 glacier surges in two spitsbergen fjords, *Quat. Sci. Rev.*, 27, 1583–1599, 2008.
- 1276 Pados-Dibattista, T., Pearce, C., Detlef, H., Bendtsen, J., and Seidenkrantz, M. S.: Holocene
1277 palaeoceanography of the Northeast Greenland shelf, *Clim. Past*, 18, 103–127,
1278 <https://doi.org/10.5194/cp-18-103-2022>, 2022.
- 1279 Pedersen, J. B. T., Kroon, A., and Jakobsen, B. H.: Holocene sea-level reconstruction in the
1280 Young Sound region, Northeast Greenland, *J. Quat. Sci.*, 26(2), 219–226, 2011.
- 1281 Rahmstorf, S., Box, J. E., Feulner, G., Mann, M. E., Robinson, A., Rutherford, S., and
1282 Schaffernicht, E. J.: Exceptional twentieth-century slowdown in Atlantic Ocean overturning
1283 circulation, *Nat. Clim. Chang.*, 5, 475–480, <https://doi.org/10.1038/nclimate2554>, 2015.
- 1284 Rasmussen, T. L., Pearce, C., Andresen, K. J., Nielsen, T., and Seidenkrantz, M.-S.: Northeast
1285 Greenland: ice-free shelf edge at 79.4°N around the Last Glacial Maximum 25.5–17.5 ka,
1286 *Boreas*, 51, 759–775, 2022.
- 1287 Reeh, N., Bøggild, C. E., and Oerter, H.: Surge of Storstrømmen, a large outlet glacier from the
1288 Inland Ice of North-East Greenland, *Rapp. Grønands Geol. Unders.*, 162, 201–209, 1994.
- 1289 Reilly, B. T., Stoner, J. S., Mix, A. C., Walczak, M. H., Jennings, A., Jakobsson, M., Dyke, L.,
1290 Glueder, A., Nicholls, K., Hogan, K. A., Mayer, L. A., Hatfield, Robert, G., Albert, S., Marcott, S.,
1291 Fallon, S., and Cheseby, M.: Holocene break-up and reestablishment of the Petermann Ice

- 1292 Tongue, Northwest Greenland, *Quat. Sci. Rev.*, 218, 322–342, 2019.
- 1293 Reimer, P. J., Austin, W. E. N., Bard, E., Bayliss, A., Blackwell, P. G., Bronk Ramsey, C.,
 1294 Butzin, M., Cheng, H., Edwards, R. L., Friedrich, M., Grootes, P. M., Guilderson, T. P., Hajdas,
 1295 I., Heaton, T. J., Hogg, A. G., Hughen, K. A., Kromer, B., Manning, S. W., Muscheler, R.,
 1296 Palmer, J. G., Pearson, C., Van Der Plicht, J., Reimer, R. W., Richards, D. A., Scott, E. M.,
 1297 Southon, J. R., Turney, C. S. M., Wacker, L., Adolphi, F., Büntgen, U., Capano, M., Fahrni, S.
 1298 M., Fogtmann-Schulz, A., Friedrich, R., Köhler, P., Kudsk, S., Miyake, F., Olsen, J., Reinig, F.,
 1299 Sakamoto, M., Sookdeo, A., and Talamo, S.: The IntCal20 Northern Hemisphere Radiocarbon
 1300 Age Calibration Curve (0-55 cal kBP), *Radiocarbon*, 62, 725–757,
 1301 <https://doi.org/10.1017/RDC.2020.41>, 2020.
- 1302 Rignot, E., Bjork, A., Chauche, N., and Klauke, I.: Storstrømmen and L. Bistrup Bræ, North
 1303 Greenland, Protected From Warm Atlantic Ocean Waters, *Geophys. Res. Lett.*, 49,
 1304 <https://doi.org/10.1029/2021GL097320>, 2022.
- 1305 Rydningen, T. A., Vorren, T. O., Laberg, J. S., and Kolstad, V.: The marine-based NW
 1306 Fennoscandian ice sheet: Glacial and deglacial dynamics as reconstructed from submarine
 1307 landforms, *Quat. Sci. Rev.*, 68, 126–141, <https://doi.org/10.1016/j.quascirev.2013.02.013>, 2013.
- 1308 Schaffer, J., von Appen, W.-J., Dodd, P. A., Hofstede, C., Mayer, C., de Steur, L., and Kanzow,
 1309 T.: Warm water pathways toward Nioghalvfjerdingsfjorden Glacier, Northeast Greenland, *J.*
 1310 *Geophys. Res. Ocean.*, 122, 4004–4020, <https://doi.org/10.1002/2016JC012462>. Received,
 1311 2017.
- 1312 Schmidt, S., Wagner, B., Heiri, O., Klug, M., Bennike, O., and Melles, M.: Chironomids as
 1313 indicators of the Holocene climatic and environmental history of two lakes in Northeast
 1314 Greenland, *Boreas*, 40, 116–130, <https://doi.org/10.1111/j.1502-3885.2010.00173.x>, 2011.
- 1315 Schoof, C. G. and Clarke, G. K. C.: A model for spiral flows in basal ice and the formation of
 1316 subglacial flutes based on a Reiner-Rivlin rheology for glacial ice, *J. Geophys. Res. Solid Earth*,
 1317 113, 1–12, <https://doi.org/10.1029/2007JB004957>, 2008.
- 1318 Shaw, J., Pugin, A., and Young, R. R.: A meltwater origin for Antarctic shelf bedforms with
 1319 special attention to megalineations, *Geomorphology*, 102, 364–375,
 1320 <https://doi.org/10.1016/j.geomorph.2008.04.005>, 2008.
- 1321 Shreve, R. L.: Esker characteristics in terms of glacier physics, Katahdin esker system, Maine.,
 1322 *Geol. Soc. Am. Bull.*, 96, 639–646, [https://doi.org/10.1130/0016-7606\(1985\)96<639:ECITOG>2.0.CO;2](https://doi.org/10.1130/0016-7606(1985)96<639:ECITOG>2.0.CO;2), 1985.
- 1324 Skov, D. S., Andersen, J. L., Olsen, J., Jacobsen, B. H., Knudsen, M. F., Jansen, J. D., Larsen,
 1325 N. K., and Egholm, D. L.: Constraints from cosmogenic nuclides on the glaciation and erosion
 1326 history of Dove Bugt, northeast Greenland, *GSA Bull.*, 1–13, 2020.
- 1327 Slabon, P., Dorschel, B., Jokat, W., Myklebust, R., Hebbeln, D., and Gebhardt, C.: Greenland
 1328 ice sheet retreat history in the northeast Baffin Bay based on high-resolution bathymetry, *Quat.*
 1329 *Sci. Rev.*, 154, 182–198, <https://doi.org/10.1016/j.quascirev.2016.10.022>, 2016.
- 1330 Smith, L. M. and Andrews, J. T.: Sediment characteristics in iceberg dominated fjords,
 1331 Kangerlussuaq region, East Greenland, *Sediment. Geol.*, 130, 11–25,
 1332 [https://doi.org/10.1016/S0037-0738\(99\)00088-3](https://doi.org/10.1016/S0037-0738(99)00088-3), 2000.
- 1333 Stacey, C. D. and Hill, P. R.: Cyclic steps on a glacial delta, Howe Sound, British Columbia,
 1334 in: *Atlas of Submarine Glacial Landforms: Modern, Quaternary and Ancient*, edited by:

- 1335 Dowdeswell, J. A., Canals, M., Jakobsson, M., Todd, B. J., Dowdeswell, E. K. & Hogan, K. A.,
1336 Geological Society of London, 93–94, 2016.
- 1337 Stocker, T. F., Qin, D., Plattner, G.-K., Tignor, M. M. B., Allen, S. K., Boschung, J., Nauels, A.,
1338 Xia, Y., Bex, V., and Midgley, P. M.: Climate Change 2013: The Physical Science Basis.
1339 Contribution of Working Group I to the Fifth Assessment Report of the Intergovernmental Panel
1340 on Climate Change, Cambridge, 2013.
- 1341 Stokes, C. R. and Clark, C. D.: Geomorphological criteria for identifying Pleistocene ice
1342 streams, *Ann. Glaciol.*, 28, 67–74, <https://doi.org/10.3189/172756499781821625>, 1999.
- 1343 Stokes, C. R. and Clark, C. D.: Palaeo-ice streams, *Quat. Sci. Rev.*, 20, 1437–1457, 2001.
- 1344 Storrar, R. D., Stokes, C. R., and Evans, D. J. A.: Morphometry and pattern of a large sample
1345 (>20,000) of Canadian eskers and implications for subglacial drainage beneath ice sheets,
1346 *Quat. Sci. Rev.*, 105, 1–25, <https://doi.org/10.1016/j.quascirev.2014.09.013>, 2014.
- 1347 Syring, N., Lloyd, J. M., Stein, R., Fahl, K., Roberts, D. H., Callard, L., and O’Cofaigh, C.:
1348 Holocene interactions between glacier retreat, sea ice formation, and Atlantic water advection at
1349 the inner Northeast Greenland continental shelf, *Paleoceanogr. Paleoclimatology*, 35, 2020.
- 1350 Wagner, B., Bennike, O., Bos, J. A. A., Cremer, H., Lotter, A. F., and Melles, M.: A
1351 multidisciplinary study of Holocene sediment records from Hjort Sø on Store Koldewey,
1352 Northeast Greenland, *J. Paleolimnol.*, 39, 381–398, <https://doi.org/10.1007/s10933-007-9120-3>,
1353 2008.
- 1354 Weber, M. E., Niessen, F., Kuhn, G., and Wiedicke, M.: Calibration and application of marine
1355 sedimentary physical properties using a mult-sensor core logger, *Mar. Geol.*, 136, 151–172,
1356 1997.
- 1357 Weidick, A., Andreasen, C., Oerter, H., and Reeh, N.: Neoglacial glacier changes around
1358 Storstrommen, north-east Greenland, *Polarforschung*, 64, 95–108, 1994.
- 1359 Wilson, N. J. and Straneo, F.: Water exchange between the continental shelf and the cavity
1360 beneath Nioghalvfjærdsbræ (79 North Glacier), *Geophys. Res. Lett.*, 42, 7648–7654,
1361 <https://doi.org/10.1002/2015GL064944>, 2015.
- 1362 Winkelmann, D., Jokat, W., Jensen, L., and Schenke, H. W.: Submarine end moraines on the
1363 continental shelf off NE Greenland - Implications for Lateglacial dynamics, *Quat. Sci. Rev.*, 29,
1364 1069–1077, <https://doi.org/10.1016/j.quascirev.2010.02.002>, 2010.
- 1365